




Article

Property Data Estimation for Hemiformals, Methylene Glycols and Polyoxymethylene Dimethyl Ethers and Process Optimization in Formaldehyde Synthesis

Steffen Schemme ^{1,2}, Sven Meschede ², Maximilian Köller ², Remzi Can Samsun ², Ralf Peters ^{2,*} and Detlef Stolten ^{3,4,5}

¹ Mitsubishi Hitachi Power Systems Europe GmbH, 47059 Duisburg, Germany; steffen_schemme@web.de

² Electrochemical Process Engineering (IEK-14), Forschungszentrum Jülich GmbH, 52425 Jülich, Germany; meschede@iuta.de (S.M.); maximilian-koeller@web.de (M.K.); r.c.samsun@fz-juelich.de (R.C.S.)

³ Techno-Economic Systems Analysis (IEK-3), Forschungszentrum Jülich GmbH, 52425 Jülich, Germany; d.stolten@fz-juelich.de

⁴ JARA-ENERGY, 52056 Aachen, Germany

⁵ Chair for Fuel Cells, Faculty of Mechanical Engineering, RWTH Aachen University, 52072 Aachen, Germany

* Correspondence: ra.peters@fz-juelich.de; Tel.: +49-2461-61-4260; Fax: +49-2461-61-6695

Received: 1 June 2020; Accepted: 29 June 2020; Published: 2 July 2020



Abstract: Polyoxymethylene dimethyl ethers (OME_n) are frequently discussed as alternative diesel fuels, with various synthesis routes considered. OME₃₋₅ syntheses demand significant amounts of thermal energy due to the complex separation processes that they entail. Therefore, innovative process designs are needed. An important tool for the development of new processes is process simulation software. To ensure sound process simulations, reliable physico-chemical models and component property data are necessary. Herein we present the implementation of a state-of-the-art thermodynamic model to describe the component systems of formaldehyde-water and formaldehyde-methanol using Microsoft[®] Excel (2010, Microsoft Corp, Redmond, WA, USA) and Aspen Plus[®], (V8.8, Aspen Tech, Bedford, MA, USA) determine the deviation between the calculated results and experimental literature data, and minimize the deviation by means of parameter fitting. To improve the accuracy of the estimation of the missing property data of hemiformals and methylene glycols formed from formaldehyde using group contribution methods, the normal boiling points were estimated based on molecular analogies. The boiling points of OME₆₋₁₀ are determined through parameter regression in accordance with the vapor pressure equation. As an application example, an optimization of the product separation of the state-of-the-art formaldehyde synthesis is presented that helps decrease the losses of methanol and formaldehyde in flue gas and wastewater.

Keywords: thermodynamic modeling; process design; Aspen Plus; power-to-fuel; synthetic fuels; formalin

1. Introduction

In replacing fossil fuels in the transport sector, one promising option is fuel synthesis via the so-called power-to-fuel (or power-to-liquid) concept [1]. In the power-to-fuel concept, H₂ produced via electrolysis powered by renewable energy and CO₂ are used to synthesize transport fuels. The required CO₂ can be captured for instance from industrial exhaust gases or ambient air. One frequently discussed alternative diesel fuel or diesel fuel additive is poly oxymethylene dimethyl ethers, which have a chain length of 3 to 5 (OME₃₋₅) [1–6]. Furthermore, OME₁ can be used as a fuel additive [7,8]. Several studies [9–16] deal with the energy demand of OME₃₋₅ synthesis based on hydrogen or methanol.

According to simulations performed by Peters [17], the direct synthesis of OME₃₋₅ from H₂ and CO₂ is, thermodynamically-speaking, virtually impossible. Although the direct synthesis of OME₁ from H₂ and CO₂ is possible under high pressures and at low temperatures, side reactions play a crucial role and a suitable catalyst would have to suppress dimethyl ether (DME) formation [17]. Further thermodynamic analyses regarding synthesis routes are published by Peters et al. [18]. The recent progress in the production of OME₃₋₅ is discussed, for instance, by Baranowski et al. [19] and Hackbarth et al. [20]. As is outlined in the literature [19–23], various synthesis routes are under discussion, wherein important intermediates along the routes include formaldehyde (FA) solutions, trioxane (TRI), DME and methylal (OME₁).

We recently published a comparative techno-economic analysis of different H₂-based production pathways towards higher alcohols, ethers including OME₃₋₅ and hydrocarbons [11]. In the course of that work, the three OME₃₋₅ synthesis routes suggested by Burger [21] were analyzed. As a result, compared to other H₂- or methanol-based production pathways towards fuels or chemicals, the OME₃₋₅ synthesis routes have the highest utility demand and, as a result, utility costs [11]. However, there is still potential for process optimization. For large-scale production in particular, the optimization of separation processes is crucial to minimizing the production costs. For process intensification and, in particular, for the challenging separation of the by-product water along the OME₃₋₅ synthesis routes, various innovative technologies are suggested, for instance integrated reaction-distillation [24], adsorption technologies using zeolites [25], pervaporation [26], thin film evaporators [12] and falling film evaporators [13]. For the correct determination of energy expenditures and the optimal design of plant components, the use of process simulation software is effective. For reliable process simulation, the component behavior and physical properties must be known and predictable using the software.

In OME_n syntheses, aqueous and methanolic formaldehyde (FA) solutions play an important role, as the water separation from FA solutions is especially energy-intensive. FA is one of the most important intermediates in the chemical industry, requiring about 50% of the methanol produced worldwide, and is commercially-available in three forms: aqueous formaldehyde solution (formalin, 35–55 wt.-%), in the form of 1-3-5-trioxane (TRI; C₃H₆O₃) and para-formaldehyde (p-FA) [27]. p-FA is polymeric FA obtained by evaporating an aqueous solution and is present with degrees of polymerization up to 100 as a thermally unstable gel and depolymerized slightly to form FA [27]. The technical handling of FA, as well as industrially-established production processes of FA from methanol, are presented by Reuss et al. [28].

FA spontaneously reacts without any catalyst with water (W) and methanol (MeOH) to form polyoxymethylene glycols (MG_n) and polyoxymethylene hemiformals (HF_n) [29–31]. MG_n and HF_n form homologous series with chain length *n*, corresponding to the number of FA components. In contrast to OME_n, MG_n and HF_n are unstable and cannot be obtained in the form of pure substances. The reaction network presented in the literature [30–35] as well as the molecular structures are shown in Figure 1. MG_n and HF_n with chain length *n* ≥ 2 have negligible vapor pressures [36,37], and so their presence can be neglected in the gas phase, as is shown in Figure 1. High FA contents lead to high degrees of polymerization, which can then lead to solid precipitation [33,37–39]. Solid precipitation occurs in solutions with >60 wt.-% FA [37] and must be avoided in technical applications, for instance by using stabilizers or small shares of methanol [28].

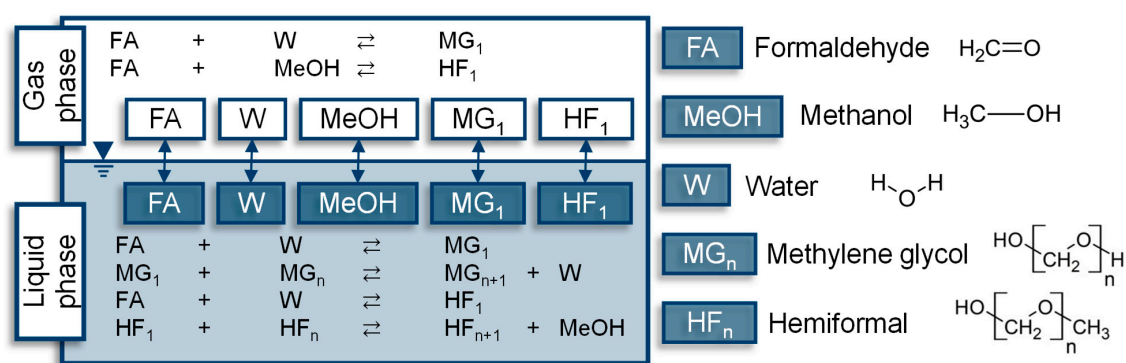


Figure 1. Chemical equilibrium reactions in water and methanol-containing formaldehyde (FA) solutions [30–35,37,39].

In recently published literature [19,24,25,29,40–42], an alternative chain growth mechanism to that shown in Figure 1 has been proposed, in which the chain length of MG_n and HF_n increases by the addition of FA. The conditions under which the individual mechanisms dominate is not clearly indicated in the literature. In process modeling, spontaneous equilibrium reactions must be considered in all process units in which FA is present, together with water and/or methanol. If the process simulation can be validated with experimental data, the mechanism of the equilibrium reactions is not directly relevant for the process design and analysis.

To determine the utility demand of separation units, thermodynamic data are required, e.g., vapor pressure, vaporization heat and heat capacity. However, in the case of OME_{n>1}, MG_n and HF_n, these data are not given the built-in property databases of process simulation programs such as Aspen Plus® and CHEMCAD. The property data of MG_n and HF_n must be estimated, as these substances do not exist in pure form and thus cannot be physically measured. The description of MG_n and HF_n as real components in the process simulation software is therefore necessary, as the reaction mechanism in the reactor depends on these components.

For robust process simulation, missing property data must be determined with experimental literature data, estimated or predicted using suitable prediction models. As stated by Ouda et al. [41], small errors in property data estimations accumulate and can affect the simulation and calculation results. Prediction models are based on the group contribution methods (e.g., Universal Quasichemical Functional Group Activity Coefficients (UNIFAC) [43], Joback [44] and Gani [45]). In general, at least the structural formulae and normal boiling points should be given for the use of property prediction models [46]. Thus, the property prediction models can be used to estimate all of the important scalar and temperature-dependent variables (i.e., critical temperature, critical pressure, vapor pressure, heat of vaporization, heat capacity, etc.) necessary for calculating material and energy balances, as well as phase equilibria. For the design of thermal separation processes, the minimum required component property data are temperature-dependent vapor pressure, heat capacity and vaporization heat.

In this paper, we discuss the deviation between calculated and experimental data using a physico-chemical system which we built-up in commercial spreadsheet software, as well as process simulation software. Another goal of this work is to develop an approach to improve the predictions of missing property data for HF_n and MG_n using group contribution methods via the estimation of normal boiling points. For the sake of completeness, the thermodynamic data of the component systems containing trioxane, DME and OME_n in process simulations are outlined through literature references or determined in the course of this paper. Another aspect is to show how the state-of-the-art FA synthesis process of the OME_{3–5} synthesis route can be optimized by recycling wastewater. In the course of that, the product of the FA synthesis is also adjusted, as different processes along the OME_{3–5} synthesis routes require different FA solutions as input material. For the sake of clarity, the research approach followed in this paper is presented in Figure 2.

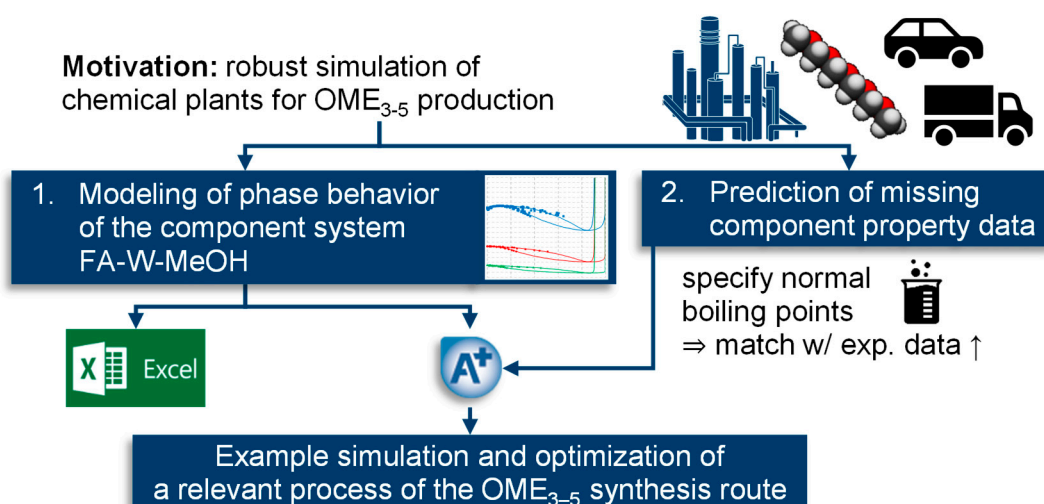


Figure 2. Illustration of the research approach followed in this paper.

2. Prior Work on Reaction Model and Property Data

In 1986, Maurer [32] described non-ideal reaction behavior in terms of activity-based equilibrium constants. Maurer [32] determined the necessary information for the UNIFAC method by drawing on the work of Gmehling et al. [47]. The fundamental physico-chemical equilibrium model developed by Maurer [32] was validated and further developed by a research group at the University of Kaiserslautern [31,33–36,48–54]. In particular, the models of Albert et al. [52] and Kuhnert et al. [33] are based on broad experimental data. The application, quality and constraints of the model published by Albert et al. [36] are discussed in O’Connell et al. [39]. Additionally, O’Connell et al. [39] modeled solid precipitation based on data from Kuhnert et al. [33,55]. As well as the equilibrium model, Hasse and Maurer [56] and Hahnenstein et al. [30] published a reaction kinetic model to describe the temperature and pH depending on HF_n and MG_n formations. This kinetic model was further developed by Ott et al. [57] and can be used in combination with the thermodynamic models of Albert et al. [52] and Kuhnert et al. [33] in process simulations of thermal separations of FA-containing component systems [57].

For use in process simulations for the basic engineering of the FA-containing processes, the further extended fundamental model published by Maurer [32] was applied by a number of companies [39], with various examples of its implementation to be found in the literature.

To determine the impact of kinetics, Grützner et al. [40] implemented two approaches using CHEMASIM software from BASF: the equilibrium model of Kuhnert et al. [33] and an advanced model that also included a reaction kinetic model, using the approach of Ott [58], which is based on the work of Hahnenstein et al. [30]. The predictions of both approaches are in good agreement with the experimental distillation data [40]. Analogously, Weidert et al. [24] showed that the implementation of the equilibrium model of Albert et al. [53] and Kuhnert et al. [33] in Matlab was also effective in predicting the experimental distillation data. Thus, referring to Grützner et al. [40] and Weidert et al. [24], the assumption that the chemical equilibrium of the component system FA-W-MeOH is reached at every distillation column stage is justified, and so the equilibrium model can be used in the process simulation. This reduces the computational effort compared to the kinetic approaches. The latest applications of the equilibrium model in the process simulations are published by Ouda et al. [59] using CHEMCAD and Ai et al. [60], Bongartz et al. [10], Burre et al. [13] and Schemme et al. [11] using Aspen Plus®.

As an alternative to property data modeling via merely group contribution models, Liu et al. [61] and Albert et al. [36] published correlations for the heat capacities of HF₁₋₁₀ (for 312–347 K) and MG₁₋₁₀ (for 323–363 K) and vapor pressures for HF₁ and MG₁ (for 293–413 K). Correlations for the

temperature-dependent enthalpy of evaporation and isobaric heat capacity of the ideal gas of OME₂₋₁₀ are published by Burger et al. [62]. For the implementation of component properties in CHEMCAD, Ouda et al. [59] estimate the heat capacities c_p of HF_{n>1}, as well as MG_{n>1}, HF₉₋₁₀ and MG₉₋₁₀ to be equal to those of the corresponding OME_n and OME₈, respectively. Bongartz et al. [10] recently published an approach to modeling the temperature-dependent enthalpies of vaporization and the ideal gas heat capacities of MG_n and HF_n based on the original model [49,61,63] to be used in Aspen Plus[®]. To comply with the assumption that the presence of HF_{n>1} and MG_{n>1} in the gas phase can be neglected, Ouda et al. [59] estimate the vapor pressures of HF_{n>1} and MG_{n>1} to be equal to those of OME₈. For the same reason, Bongartz et al. [10] set the normal boiling points of HF_{n>1} and MG_{n>1} at 1000 K and calculated the critical points of HF_n and MG_n using the group contribution from Ott [58].

3. Modeling Approaches and Discussion of the Results

In this section, the required methodology is developed and implemented according to the research design presented in Figure 2. Firstly, the numerical approaches to describe the chemical model are developed in Section 3.1 to prepare the basis for process simulations. This is followed by Section 3.2, which deals with the estimation of missing property data. The developed methods and their outcome flow into Section 3.3., in which a process optimization is practiced for the selected example of formaldehyde synthesis.

3.1. Development of the Chemical Model

To ensure sound process simulation design, as a first step, a physico-chemical system is simulated by means of a numerical approach using Microsoft[®] Excel to illustrate the phase equilibria of FA-W and FA-MeOH and create a fundamental understanding of the component system.

The modeling of the reaction network shown in Figure 1 is based on the work of Maurer [32], which is state-of-the-art and describes the reactions and component distribution with activity-based equilibrium constants using the UNIFAC method [43], linked to the extended Raoult's law to model the gas phase. The model, drawn from Maurer [32] and describing the activity coefficients, is presented in the Appendix A (see Equation (A1) to (A4)). The necessary data of the molecular groups of W, FA, MeOH, HF_n and MG_n required by the UNIFAC method are also noted in Maurer [32]. The molecular groups CH₂(OH)₂ and CH₂OH are not standard groups of the UNIFAC method. The phase equilibria depending on the mole fractions of FA-W and FA-MeOH can be determined by calculating the stoichiometric mole fractions using the reaction equations as described by Albert et al. [52] (see Equation (A5) to (A8) in the Appendix A).

In the following sub-section, firstly the numerical approach will be developed. Afterwards, the developed chemical model will be implemented in process simulation software. As the last step, the remaining component systems trioxane, DME, OME_n are given for the sake of completeness.

3.1.1. Numerical Approach for Formaldehyde-Containing Component Systems

In the numerical approach, the UNIFAC method [43] for calculating the activity coefficients is implemented in Microsoft[®] Excel and logically linked to the volume, surface and interaction parameters drawn from the work of Maurer [32]. Additionally, the correlations for the equilibrium constants given by Maurer [32] (Equation (1)) and mass balances (Equations (A5) to (A8)) given by Albert et al. [52] to recalculate the FA, W and MeOH shares were implemented.

$$\ln(K_{i,n}) = A + \frac{B}{T/K} + \frac{C}{(T/K)^2} \quad (1)$$

The correlation between the UNIFAC method, which uses the equilibrium composition of the liquid phase to predict the activity coefficients γ_i , and the correlation for the equilibrium constant, which in turn determines the equilibrium composition using the activity coefficient, results in a circular

dependency. As a starting point, the activity coefficients are set to $\gamma_i = 1$. As a termination criterion, the activity of water γ_W was chosen. According to Equation (2), the relative deviation e of two successive iterations ($z - 1$ and z) should fall below a specific value. For convergence, the maximum relative deviation was set to $e = 0.1\%$:

$$\left| \frac{\gamma_{Wz} - \gamma_{Wz-1}}{\gamma_{Wz}} \right| \leq e \quad (2)$$

The numerical solution is complicated by unstable target values that permanently decay into two thermodynamically-inconsistent but stable points, which cannot represent the experimental data. Therefore, an additional convergence strategy was used to allow the unstable point to be transformed into a stable point according to Equation (3):

$$\gamma_{iz} = 0.5 \gamma_{iz-1} + 0.25 \gamma_{iz-2} + 0.25 \gamma_{iz-3} \quad (3)$$

Figures 3 and 4 show the pressure-dependent phase equilibria for the component systems FA-W and FA-MeOH that were determined with the implemented approach compared to the experimental literature data [32,34,64,65] (with 72 data points for FA-W and 27 data points for FA-MeOH). Maurer [32] suggests a maximum oligomer chain length of $n = 30$. As in the works of Ott [58], Ouda et al. [41] and Bongartz et al. [10], in this work the maximum chain length is set to $n = 10$ to reduce computational requirements. As Figures 3 and 4 show, calculations with the maximum chain length of $n = 10$ are sufficient to get very close to the experimental data.

The vapor pressures in the component systems FA-W and FA-MeOH remain low over a wide molar range of FA and are even smaller with increasing FA content. The reason for this is the continuous reactions of FA to long-chain oligomers, which have a lower vapor pressure. The reaction occurs until all the water has reacted to the methylene glycols and methanol to hemiformal and is no longer present in the equilibrium state. Therefore, the oligomerization reactions in more concentrated FA solutions can no longer take place where monomeric FA is present. The monomeric FA evaporates, significantly increasing the vapor pressure. An azeotropic point exists for both material systems, with an FA content of about 85 mol.-%. At 90 °C and 70 °C, the FA-W system also has more azeotropes at FA levels of 12 mol.-% and 2 mol.-%, which is not directly apparent in Figure 3.

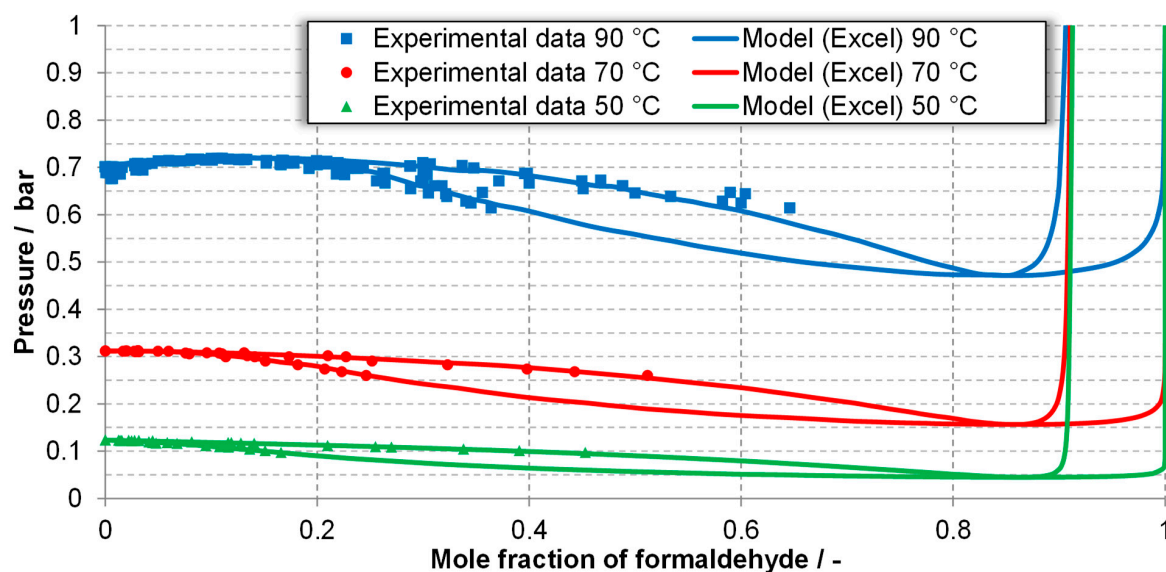


Figure 3. Phase equilibrium of the system formaldehyde-water (FA-W) for different temperatures calculated using Excel and compared to the experimental data [32,34,64,65].

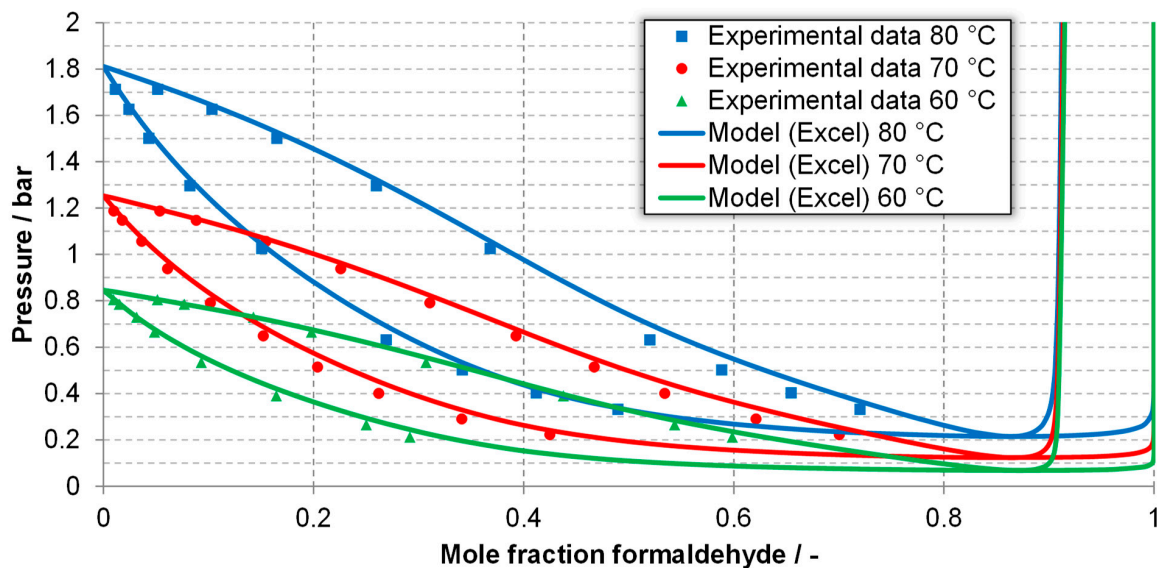


Figure 4. Phase equilibrium of the system formaldehyde-methanol (FA-MeOH) for different temperatures calculated using Excel compared to the experimental data [65].

Table 1 shows the average of the relative deviations of pressure and temperature ($ARD_{p,T}$; see Equation (4)) and the standard deviations ($s_{p,T}$; see Equation (5)) of the modeled phase equilibria diagrams shown in Figures 3 and 4 to the 99 experimental data points given in the diagrams. In each case, the values are determined for the dew point and boiling point line of the component system.

$$ARD_{p,T} = \frac{1}{m} \sum_{i=1}^m \left(\left| \frac{p, T_{m_{exp.}} - p, T_{m_{model}}}{p, T_{m_{exp.}}} \right| \right) \quad (4)$$

$$s_{p,T} = \sqrt{\frac{1}{m} \sum_{i=1}^m \left(\left| \frac{p, T_{m_{exp.}} - p, T_{m_{model}}}{p, T_{m_{exp.}}} \right| - ARD_{p,T} \right)^2} \quad (5)$$

Table 1. Average of the relative deviations (ARD) and standard deviations between the modeled phase equilibria diagram shown in Figures 3 and 4 and the experimental data [32,34,64,65].

Component System		Diagram of the Modeled Phase Equilibria and Experimental Data	Boiling Point Line		Dew Point Line	
			ARD %	s %	ARD %	s %
FA-W system generated using Excel	90 °C	Figure 3, experimental data [32,34,64,65]	1.23	1.27	1.17	0.86
	70 °C		0.65	0.63	0.57	0.41
	50 °C		0.48	0.53	0.69	0.47
FA-MeOH system generated using Excel	80 °C	Figure 4, experimental data [65]	6.43	5.35	3.40	2.73
	70 °C		6.30	5.63	6.34	4.47
	60 °C		3.36	3.88	5.45	5.35

The processes in aqueous and methanol-containing formaldehyde solutions can be even better clarified with the equilibrium distributions of the oligomers MG_n and HF_n , as is shown in Figures 5 and 6. For recalculated FA mole fractions of 0–90 mol.-%, monomeric FA is present in the corresponding equilibrium state with only a maximum of 10 mol.-%, while the remaining fraction is polymerized. The corresponding equilibrium distributions in the gas phase are given in Figures A1 and A2 in the Appendix A. For a recalculated FA content of ca. 91 mol.-%, the entire water content is bound in the oligomers. Therefore, as is shown in Figures 5 and 6, in both component systems the content of MG_{10} or HF_{10} in equilibrium in this case reached the maximum with a value of more than 60 mol.-%.

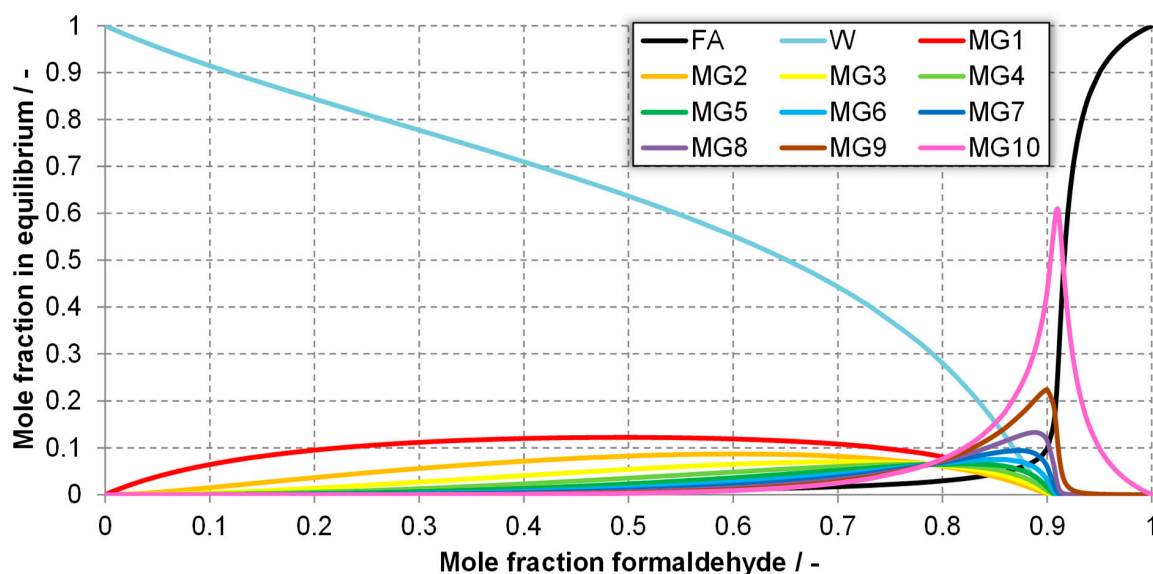


Figure 5. Equilibrium distribution in the liquid phase of the component system FA-W at 90 °C.

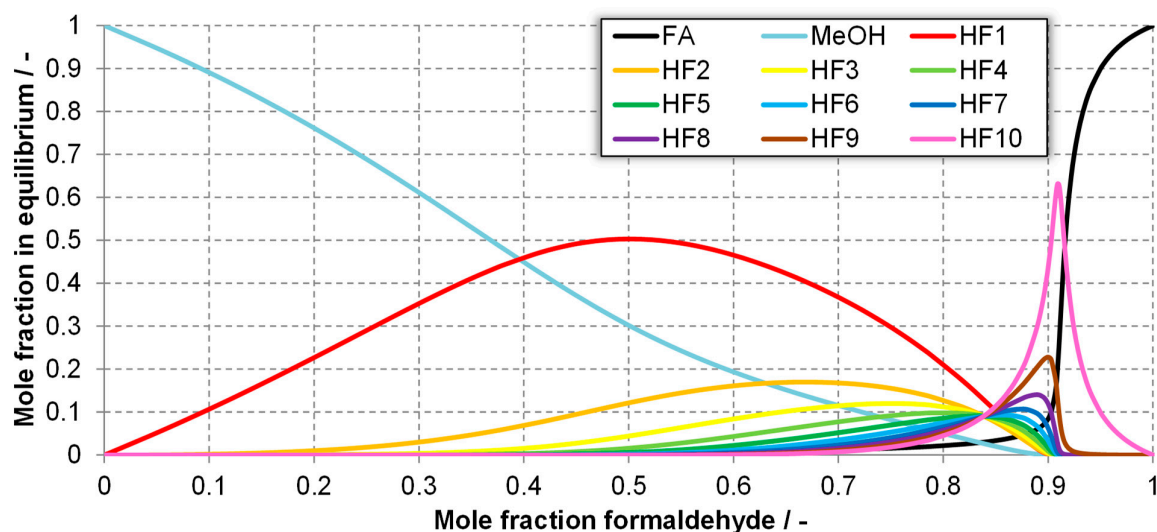


Figure 6. Equilibrium distribution in the liquid phase of the component system FA-MeOH at 80 °C.

Generally, however, such high FA contents are not technically relevant, as otherwise the long oligomers precipitate as solids. Ott et al. [37], state that solids precipitate in FA-W and FA-MeOH solutions with > 60 wt.-% FA (corresponding to 47.4 mol.-% FA in FA-W and 61.5 mol.-% FA in FA-MeOH).

According to the equilibrium distributions shown in Figures 5, 6, A1 and A2, the formation of HF₁ in the FA-MeOH system is significantly stronger than that of MG₁ in the FA-W system. Therefore, in technical applications, methanol is often added to aqueous FA solutions to suppress the formation of long-chain MG_n with high melting points [28,66]. This leads to the stabilization of the oligomerization reactions and thus to inhibited solid precipitation. In general, the formation of HF_n and MG_n is favored by high overall levels and low temperatures [66].

Knowledge regarding the mole fraction distribution can, depending on the FA content and temperature, help optimize the operation of the reactors. For example, FA-based trioxane is formed by means of linear MG₃ [67] or MG_{n ≥ 3} [68]. Maximizing the share of MG₃ or MG_{n ≥ 3} by varying the operating conditions and FA share has the potential to increase the trioxane yield. Another, analogous example is the acid-catalyzed reaction of methanol and HF₁ to OME₁ [24,29,69].

In this sub-section, it is shown that the developed chemical model can reproduce the experimental results with a high accuracy. In the next sub-section, the model will be implemented in process simulation software.

3.1.2. Implementation of the Chemical Model in Aspen Plus®

The UNIFAC method and its equations are already implemented by default in Aspen Plus®. The volume, surface, and interaction parameters, drawn from the work of Maurer [32], are implemented using the available template. The input format of the Chemistry template of Aspen Plus®, which is used to describe the equilibrium reactions shown in Figure 1, corresponds to Equation (6) and is, thus, mathematically consistent with the equation given by Maurer [32] (Equation (1)).

$$\ln(K) = A + \frac{B}{T} + C \cdot \ln(T) + D \cdot T \quad (6)$$

The parameters for the implementation of the temperature-dependent equilibrium constants are determined by a parameter fitting based on the least squares method (Gauss [70]). The error sum of squares (LSE) is minimized for all relevant equilibrium constants, in accordance with Equation (7):

$$LSE_i = \sum_{T=273.15 \text{ K}}^{373.15 \text{ K}} \left[\ln\left(K_{i,\text{Equation}(1)}^L(T)\right) - \ln\left(K_{i,\text{Equation}(6)}^L(T)\right) \right]^2 \quad (7)$$

The parameter fitting is carried out in the temperature range 0–100 °C, which is relevant for the OME_{3–5} syntheses. The respective parameters of Equation (6) are varied to minimize the least square error (LSE) for the considered component. Additionally, a curve-fitting method was applied to K_{HF_1} and K_{MG_1} , so that the phase equilibria better match the experimental data. The formation of MG_1 and HF_1 has the greatest influence on the phase equilibrium, which is why the associated correlation parameters are most suitable for influencing the calculated phase equilibria. Table 2 shows the determined correlation parameters for use in the Aspen Plus® template. Due to the applied curve-fitting, the LSE of $\ln(K_{\text{HF}_1}^L)$ and $\ln(K_{\text{MG}_1}^L)$ are relatively larger than the others.

Table 2. In Aspen Plus®, with the implemented correlation parameters of the equilibrium constants and least square errors (LSEs).

n	$\ln(K_{\text{MG}_n}^L)$				$\ln(K_{\text{HF}_n}^L)$			
	A	B	C	LSE	A	B	C	LSE
1	−242.1	17180	33.547	3.131	73.85	600	−11.7	1.945
2	151.9215	−8666.63	−21.5084	0.230	−2.097	−49.15	0.0	0.0
3	152.41	−8508.3	−21.7035	0.259	−1.635	−53	0.0	0.0
4	152.372	−8502.62	−21.6948	0.199	−1.682	−53	0.0	0.0
5	152.367	−8491.15	−21.6964	0.200	−1.709	−53	0.0	0.0
6	152.363	−8470.65	−21.7035	0.252	−1.728	−53	0.0	0.0
7	152.358	−8470	−21.7015	0.232	−1.741	−53	0.0	0.0
8	152.351	−8477	−21.696	0.187	−1.751	−53	0.0	0.0
9	152.334	−8468.75	−21.6961	0.205	−1.759	−53	0.0	0.0
10	152.3375	−8464.4	−21.698	0.216	−1.765	−53	0.0	0.0

In the original model of Maurer [32], the gas phase was modeled as ideal gas. In this work, the gas phase is modeled using the Redlich-Kwong state equation for real gases [71] to enable the modeling of phase behavior at higher pressure. The phase diagrams of FA-W and FA-MeOH, generated after implementing the new thermodynamic and chemistry data using Aspen Plus®, are shown in Figures 7 and 8, together with experimental literature data [32,34,64,65].

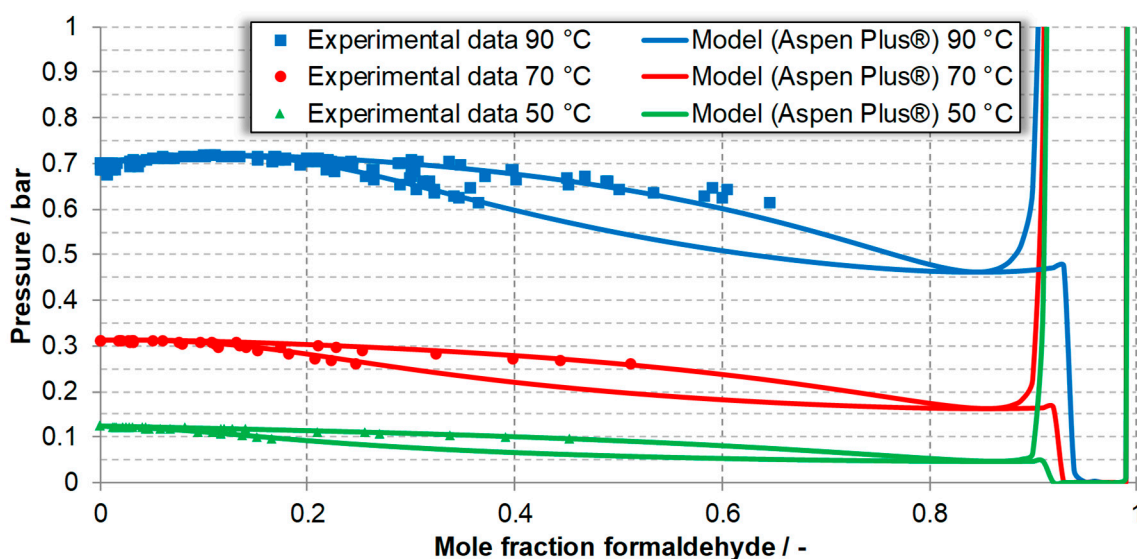


Figure 7. Phase equilibrium of the FA-W-system for different temperatures calculated using Aspen Plus®, compared to the experimental data [32,34,64,65].

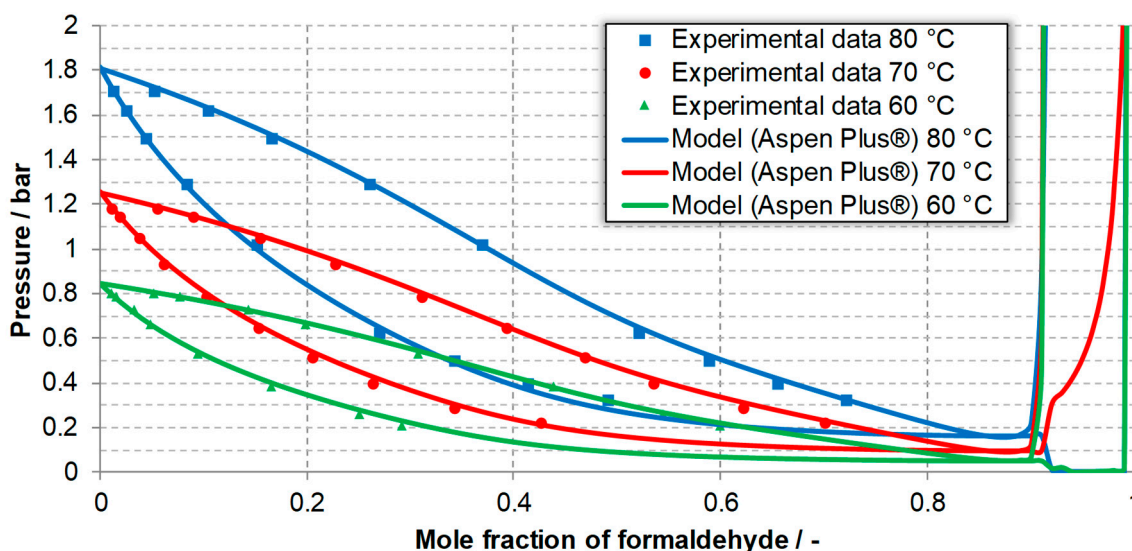


Figure 8. Phase equilibrium of the FA-MeOH system for different temperatures calculated using Aspen Plus®, compared to the experimental data [65].

The two diagrams generated using Aspen Plus, which are shown in Figures 7 and 8, are broadly consistent with the diagrams generated with Microsoft® Excel (Figures 3 and 4). Comparing the values given in Tables 1 and 3, the experimental literature data of the FA-MeOH component system can be even better described using the Aspen Plus® model, which is achieved by slightly adjusting the correlation parameters. Discrepancies only occur in the area of the stoichiometric FA shares of >85 mol.-%, where the vapor pressures are in part 0 bar. The Aspen Plus® solver algorithms appear to have convergence issues in this region. However, this is acceptable because FA shares of >85 mol.-% are not reached on the OME_n synthesis routes and so the phase behavior for compositions relevant for process simulations is modeled with sufficient accuracy.

Table 3. Average of the relative deviations and the standard deviations between the modeled phase equilibria diagram shown in Figures 7 and 8, as well as the experimental data.

Component System	Diagram of Modeled Phase Equilibria and Experimental Data	Boiling Point Line		Dew Point Line		
		ARD %	s %	ARD %	s %	
FA-W system generated using Aspen Plus®	90 °C	Figure 7,	1.29	1.48	1.66	1.25
	70 °C	Experimental data	0.74	0.74	0.57	0.38
	50 °C	[32,34,64,65]	0.43	0.41	1.23	0.90
FA-MeOH system generated using Aspen Plus®	80 °C	Figure 8,	1.88	1.83	3.77	4.88
	70 °C	experimental data [65]	2.52	2.55	3.07	2.40
	60 °C		1.50	1.39	2.88	3.04

With this step, the chemical model is not only transferred to process simulation software for performing detailed analyses, but also the accuracy level is further increased.

3.1.3. Other Components Systems: Trioxane, Dimethyl Ether (DME), Polyoxymethylene Dimethyl Ethers (OME_n)

The UNIFAC parameters required to describe the component systems of FA-W and FA-MeOH, including MG_n and HF_n, are given by Maurer [32]. These component systems only cover a part of all occurring component systems on the OME_n synthesis routes, albeit the far more thermodynamically-complex ones. In contrast to FA, trioxane, DME and OME_n exhibit no additional spontaneous reaction mechanisms, which is why only the corresponding UNIFAC parameters must be implemented.

For the sake of completeness, the corresponding UNIFAC groups and UNIFAC parameters are listed in Tables A2–A4 in the Appendix A. As can be seen from Table A2, trioxane and methylal are modeled as autonomous UNIFAC groups. The corresponding values can be taken from Grützner [72] (based on Albert [49]) and Drunsel [29] (based on Kuhnert [73]). For the description of OME_n, Schmitz et al. [54] introduced a second oxymethylene group (-CH₂O-)OME that resembles the existing oxymethylene group (-CH₂O-), but has changed the interaction parameters with water and methylal on the basis of experimental data. For use in Aspen Plus®, the interaction parameters must be reduced to scalar values. An appropriate temperature, based on the temperature levels of the varied synthesis steps in the work of Burger [21], Oestreich [22], Grützner [72] and Drunsel [69], is 353.15 K. The selected values can be adjusted as required; however, the influence is relatively low and the resulting deviations with respect to the present temperature ranges are therefore justifiable.

The UNIFAC parameters of the trioxane-methylal component system are not available, but can be determined via regression as per the work of Burger [21], who described the system using the NRTL (non-random two-liquid) method (the results are displayed in Table A1 in the Appendix A for the sake of completeness).

The DME-containing component systems occurring on the OME_{3–5} synthesis routes have been neither sufficiently studied nor thermodynamically-modeled. However, reliable thermodynamic data are required for process design and simulation, for instance for the formation of OME_{3–5} from DME and trioxane [74]. Two different approaches are possible in terms of the UNIFAC parameters of DME: decomposition into existing UNIFAC groups (CH₃O- and -CH₃) and the use of an autonomous UNIFAC group (C₂H₆O). In some cases, decomposition into existing UNIFAC groups insufficiently reproduces experimental data. For instance, the miscibility gap in the component system DME-W cannot be sufficiently described. Modeling as an autonomous UNIFAC group requires further unknown UNIFAC parameters that can be adapted to the existing data. However, the data are not sufficient to consider all occurring material systems of the OME_{3–5} synthesis routes. Thus, the missing UNIFAC parameters cannot be added and are set as equal to zero which, according to the UNIFAC method, corresponds to an ideal liquid phase. For process simulations where all components are given in the default database of the process simulation software, such as DME synthesis from methanol, other thermodynamic models such as NRTL should be used.

3.2. Estimation of Property Data of OME_{2–10}, Polyoxymethylene Glycols (MG_n) and Hemiformals (HF_n)

In this section, an approach to estimating the missing component property data for OME_{2–10}, MG_n and HF_n is presented. The estimation is carried out using the group contribution method PCES (Property Constant Estimation System) from Aspen Plus®.

Prior to this, to determine the accuracy of a property estimation system, the relative deviations of the property data of OME₁, DME (dimethyl ether) and TRI (trioxane), estimated using PCES (property constant estimation system [75,76]), as well as property data from the Aspen Plus® databases, were determined. In case 1, only the molecular structure is given. In case 2, the inputs for the property estimation system are the molecular structure and normal boiling point. The results are given in Table 4. In case 1, the normal boiling point T_B is also estimated with group contribution methods that use the molecular structure. The estimations are performed with the JOBACK method [44].

Table 4. Comparison of critical component properties from Aspen Plus® databases with the built-in predictive models.

	Aspen Plus® Database			Case 1: Estimation Using the Molecular Structure			Case 2: Estimation Using the Molecular Structure and Boiling Point T _B		
	T _B /K	T _C /K	p _C /bar	T _B /K ARD/%	T _C /K ARD/%	p _C /bar ARD/%	T _B /K ARD/%	T _C /K ARD/%	p _C /bar ARD/%
OME ₁	315.0	497.0	39.5	312.9 0.7%	477.4 3.9%	42.2 6.8%	315.0 0.0%	480.7 3.3%	42.2 (6.8%)
DME	248.3	400.0	53.7	267.6 7.8%	427.9 7.0%	49.1 8.6%	248.3 0.0%	397.2 0.7%	49.1 (8.6%)
TRI	387.7	604.0	58.2	373.1 3.8%	585.0 3.2%	59.6 2.5%	397.7 0.0%	607.8 0.6%	59.6 (2.5%)

The reference values used are the critical temperature T_C and critical pressure p_C, as these are applied to many equations of state (e.g., Redlich–Kwong, Peng–Robinson, Van der Waals), which are in turn utilized to describe thermodynamic systems. Other missing component properties, such as the vapor pressure or enthalpy of vaporization, can be estimated with the RIEDEL method based on T_B, T_C and p_C and, respectively, the LI-MA method based on the structure and T_B [76].

The relative deviations of the estimated data to the data from the database are indicated below the estimated data. Referring to Table 4, different degrees of deviations must be expected (here: up to 8.56%). T_C is calculated using the JOBACK method based on the molecular structure and T_B. p_C is exclusively calculated based on the molecular structure, which is why the respective values are equal in both case 1 and case 2. The relative deviation for the T_C can be reduced if the normal boiling point is given. This result underlines the recommendation that, at a minimum, the molecular structure as well as the normal boiling point should be conveyed in order to reliably estimate data. In the following sub-sections, the normal boiling points of OME_n, MG_n and HF_n are estimated and finally the critical temperatures of these compounds are estimated based on normal boiling points and molecular structures.

3.2.1. Estimation of the Normal Boiling Points of OME_n

Boyd [77] experimentally determined the vapor pressures of OME_{2–5} and correlated them according to the temperature (Equation (8)), which can then be used to determine the normal boiling points T_B.

$$\ln\left(\frac{p}{\text{kPa}}\right) = A + \frac{B}{T/\text{K} + C} + D \cdot \ln(T/\text{K}) \quad (8)$$

To calculate the missing T_B of OME_{6–10}, a linear regression was performed using the correlation parameters given by Boyd [77]. The corresponding diagrams are given in the Appendix A (Figures A4–A6). The parameters for OME₃ are identified as a discrepancy and not considered for the regression.

Table 5 lists the given and calculated correlation parameters of the vapor pressure equation (Equation (8)) and the normal boiling points for OME_{2–10}, which are implemented in Aspen Plus® to use the internal prediction method PCES to model the component data, which is not given in literature.

Table 5. Correlation parameters of vapor pressure equation (Equation (8)) and the normal boiling points of OME_n.

OME _n Chain Length n	A	B	C	D	T _B /°C	Reference
2	75.01	−7223.44	0.0	−8.25	104.7	[77]
3	70.59	−8042.31	0.0	−7.41	155.6	[77]
4	88.12	−10017.28	0.0	−9.75	201.3	[77]
5	93.85	−11323.17	0.0	−10.40	241.7	[77]
6	100.40	−12720.00	0.0	−11.15	276.6	*
7	106.72	−14091.90	0.0	−11.87	307.9	*
8	113.04	−15462.80	0.0	−12.59	335.7	*
9	119.36	−16833.70	0.0	−13.31	360.7	*
10	125.67	−18204.60	0.0	−14.03	383.1	*

* Linear regression (based on data provided by Boyd [77]).

3.2.2. Estimation of the Normal Boiling Points of MG_n and HF_n

Table A5 in the Appendix A gives the normal boiling points T_B of MG_{1–10} and HF_{1–10} based on the molecular structure estimated with the PCES (JOBACK method). The group contribution method predicts a constant increase of 45.3 K for each additional oligomerization unit of an oxymethylene group (−CH₂O−). However, MG_n and HF_n have a similar molecular structure to OME_n and the latter shows no linear increase as a function of length (see Table 5).

The T_B of MG₁ and HF₁ can be calculated using the parameters given by Maurer [32], who correlated the vapor pressures of MG₁ and HF₁ with the vapor pressure equation (Equation (8)) using a UNIFAC model (see Table 6).

Table 6. Correlation parameters of the vapor pressure equation (Equation (8)) and normal boiling points (T_B) of HF₁ and MG₁.

	A	B	C	D	T _B /°C	Reference
MG ₁	11.0768	1997.20	−142.72	0.0	178.8	[32]
HF ₁	18.0125	5125.00	0.0	0.0	109.5	[32]

Referring to Tables A5 and 6, the values estimated with the PCES method differ significantly from those calculated with the data given in Maurer [32]. The prediction of the T_B of MG_n and HF_n via the PCES method using merely the molecular structure is, therefore, not advisable, which is why a different approach is chosen. It is assumed that the T_B of MG_n and HF_n increase with each oligomerization unit (−CH₂O−), analogous to those of OME_n (see Equation (9)).

$$T_B(\text{OME}_n) - T_B(\text{OME}_{n-1}) = T_B(\text{MG}_n) - T_B(\text{MG}_{n-1}) = T_B(\text{HF}_n) - T_B(\text{HF}_{n-1}) \quad (9)$$

Applying Equation (9) and the values given in Table 6 results in the T_B for MG_{1–10} and HF_{1–10} listed in Table 7.

Table 7. Calculated normal boiling points (T_B) of MG_{1–10} and HF_{1–10}.

T _B /°C	n = 1	n = 2	n = 3	n = 4	n = 5	n = 6	n = 7	n = 8	n = 9	n = 10
MG _n	178.8	241.6	292.5	338.3	378.6	413.6	444.8	472.7	497.6	520.1
HF _n	109.5	172.3	223.2	268.9	309.3	344.3	375.5	403.4	428.3	450.8

The critical temperatures T_C of MG_n , HF_n and OME_n , which were estimated based on the normal boiling point T_B and the molecular structure, are given in Table 8.

Table 8. Estimated critical temperature (T_C) of MG_{1-10} , HF_{1-10} and OME_{1-10} .

$T_C/^\circ\text{C}$	n = 1	n = 2	n = 3	n = 4	n = 5	n = 6	n = 7	n = 8	n = 9	n = 10
MG_n	356.9	400.1	443.3	486.9	531.3	577.0	624.2	673.3	724.9	779.3
HF_n	282.8	327.4	371.3	415.0	458.9	503.4	549.0	596.1	645.0	696.1
OME_n	223.9 *	280.7	333.2	377.5	414.4	442.9	469.4	493.2	515.1	536.0

* Value given in Aspen Plus® database.

3.3. Simulation and Optimization of Formaldehyde Synthesis

In this section, we present an optimized concept of the state-of-the-art FA synthesis, which is possible to perform when the methanol-based FA synthesis is part of an OME_{3-5} production route. In the conventional processes, the FA solution is separated from the reactor product via an absorption column using pure water as the absorbent and, depending on the process concept, an additional downstream distillation column.

As is shown in the following, due to the use of water with a small share of FA as the absorbent instead of pure water, it is possible to decrease the MeOH loss in the absorber top stream, as well as the loss of FA that is chemically bound in wastewater. Additionally, the wastewater treatment and freshwater demand are reduced. Consequently, the raw material requirement is reduced, and the overall yield and efficiency of the OME_{3-5} synthesis routes is increased.

In the following, an application example is described to show the impact of the optimization on the process efficiency and yield. The exemplary process design of an FA synthesis is developed on the basis of the silver catalyst process with incomplete methanol conversion of the chemical company ICI (Imperial Chemical Industries), which is similar to the BASF process and outlined by Reuss et al. [28] and Chauvel and Levebre [78].

Figure 9 shows the three OME_{3-5} synthesis routes that are suggested by Burger [21] and techno-economically analyzed and compared by Schemme et al. [11]. As different processes on the OME_{3-5} synthesis routes require aqueous FA solutions with varying methanol contents, the routes are slightly modified. The discussed FA process, as well as the OME_1 and TRI process to which reference is made, correspond to those used in the techno-economic analysis of Schemme et al. [11].

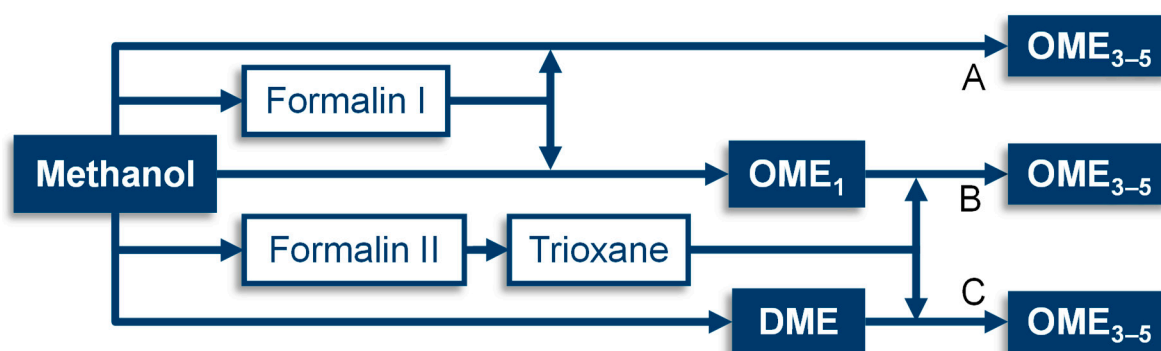


Figure 9. Poly oxymethylene dimethyl ethers with a chain length of 3 to 5 (OME_{3-5}) synthesis routes based on methanol (reproduced with modifications; Burger [21]).

In contrast to the TRI synthesis [40,72], which requires methanol-free FA solutions (formalin II), in the OME_1 synthesis and the direct OME_{3-5} from formaldehyde and methanol, the separation of unconverted methanol (distillation recovery of methanol [28]) from the reactor product can be omitted. The process flowsheet is given in Figure 10, which combines the synthesis of two different FA solutions:

formalin I and formalin II. In the simulation model, the chemical reactions from MeOH to FA taking place in the reactor R-1 are described using the kinetic model of Panzer and Emig [79], which considers the following reactions, Equations (10) to (13).

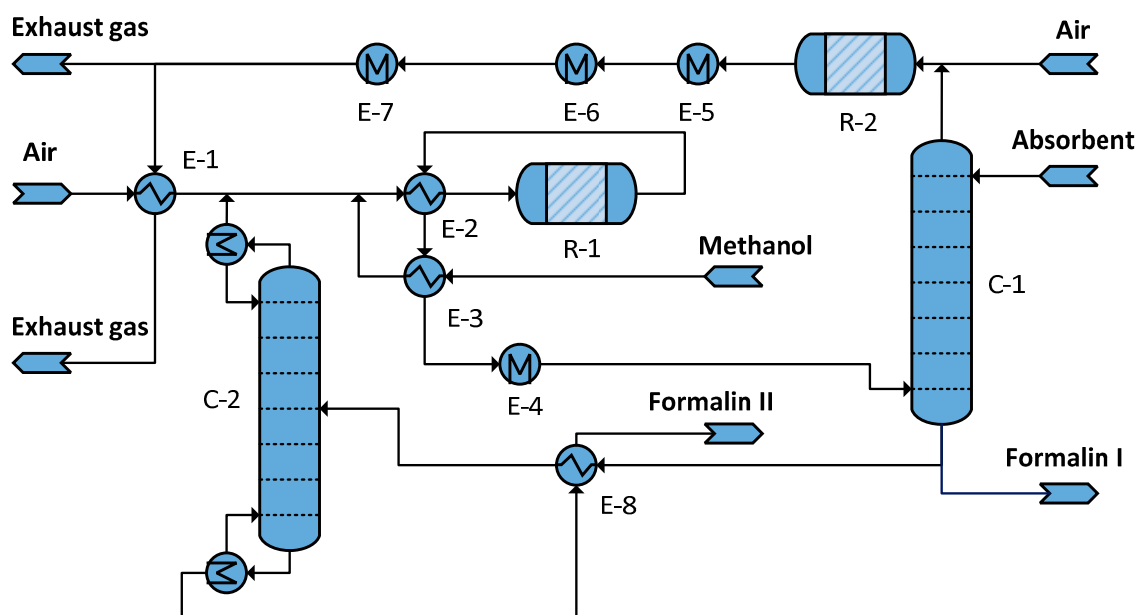
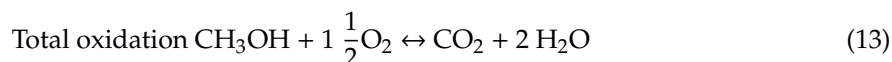
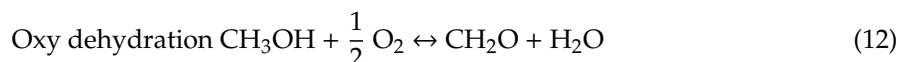
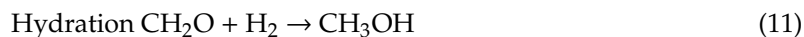
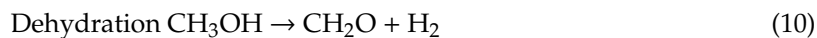


Figure 10. Process flowsheet for formalin synthesis from methanol.

Table 9 gives the Gibbs free energy (ΔG_R) and enthalpy of reaction (ΔH_R) of the reaction Equations (10) to (13) for ideal gas states under standard conditions (STP) and calculated using the PSRK (Predictive Soave–Redlich–Kwong) model at reaction conditions of 630 °C and 1 bar.

Table 9. Gibbs free energy (ΔG_R) and enthalpy of reaction (ΔH_R) of the reaction Equations (10) to (13).

Equation	ΔG_R^{STP} kJ/mol	ΔH_R^{STP} kJ/mol	$\Delta G_R^{react. cond.}$ kJ/mol	$\Delta H_R^{react. cond.}$ kJ/mol
Equation (10)	52.63	85.33	−19.73	92.05
Equation (11)	−52.63	−85.33	19.73	−92.05
Equation (12)	−176.14	−156.67	−217.82	−155.35
Equation (13)	−689.57	−676.46	−720.34	−673.22

By using the kinetic model of Panzer and Emig [79], sensitivity analyses reveal that an increased O_2/MeOH ratio increases the methanol conversion, but also reduces the selectivity towards FA. The maximum FA yield is achieved with an O_2/MeOH ratio at 0.25 mol/mol. This ratio provides an optimal balance between FA formation and ongoing oxidation. Possible side reactions such as the formation of formic acid are largely suppressed at temperatures of 590–650 °C [28] and are therefore neglected in the simulation. As the highest MeOH conversion is not reached in the chemical equilibrium, the residence time is limited and the reactor outlet stream is immediately quenched after leaving the catalyst bed. The stoichiometric FA share in the reactor product is 21.5 wt.-%. After cooling down,

the FA solution is separated from gaseous components using an absorber column (C-1 in Figure 10). In the case of formalin II synthesis, methanol is separated in distillation column C-2 and recycled back (distillation recovery of methanol [28]). For the synthesis of formalin I, C-2 is not required, and the bottom product of C-1 can be used directly as input for the following process. Due to the incomplete methanol conversion, formalin I has a stoichiometric methanol share of 18.6 wt.-% and equal FA and water shares by weight.

The amount of absorbent used in C-1 is adjusted so that the mass ratio of FA/W in the bottom outlet is 1. A slight loss of volatile methanol in the top stream of the absorber C-1 is unavoidable. If pure water is used as the absorbent (base case), up to 1.65% of the methanol (stoichiometric) supplied to the process or, respectively, 6.3% of the methanol (stoichiometric) fed into the absorber leaves the process with the absorber top stream. If water with a small share of FA is used as the absorbent, the FA causes the methanol to be bound in the form of hemiformals in the liquid phase according to the reaction network shown in Figure 1. The methanol loss can be more than halved if wastewater from the downstream OME₁ synthesis with a stoichiometric FA content of 5.2 wt.-% is used instead of fresh water. The stoichiometric FA content of 5.0 wt.-% means an FA loss of 0.04 kg_{FA}/kg_{OME1}.

Even the use of the wastewater of the TRI synthesis with a stoichiometric FA content of about 1.0 wt.-% used as the absorbent reduces the loss of methanol. With both TRI and OME₁ production, the amount of wastewater is higher than the amount of absorbent required. In the example simulation described, 42% of the wastewater of the OME₁ is required to cover the absorbent demand of the corresponding FA synthesis.

As reported by Reuss et al. [28], the gaseous top stream is burned using air. The waste heat can be used to produce steam to support covering the heat demand of other processes. The product distribution and reaction heat (reactor R-2 in Figure 10) is determined by minimizing the Gibbs free energy (Aspen Plus[®] reactor model *RGibbs*). With a high surplus of air ($\lambda \approx 2.5$) resulting in a combustion temperature of 800 °C, the NO_x content in the exhaust gas is around 100 mg/m³ (norm cubic meter, water free). For heat supply and recovery, saturated steam at three different temperature levels (250 °C, 175 °C and 125 °C) is used within the simulation, leading to a slight limitation compared to heat integration via pinch analysis, but is closer to the technical implementation.

Figure 11 shows the temperature-depending phase equilibria of the binary systems W/FA and W/MeOH, corresponding to Figures 3 and 4, as well as the phase diagram of W/MeOH in a prism illustration. To elucidate the effect of vapor-liquid equilibria data on the separation behavior of the distillation column C-2 in Figure 10, the corresponding conodes were depicted in a phase diagram (see Figure 11). For ease of understanding Figure 11, the binary diagrams of the system W/MeOH/FA without conodes is given in Figure A3 in the Appendix A. The phase diagram in Figure 11 shows a small region for vapor-liquid phase separation due to the formation reactions of hemiformals and methylene glycols in the W/MeOH/FA system. The phase equilibria at constant pressure shown in Figure 11 is overwhelmed by the azeotrope at high FA concentrations in combination with the high saturation pressure of the pure species and the low boiling temperature. Additionally, solid precipitation must be considered at high FA concentrations, (see Ott et al. [57]). The design of column C-2 in Aspen Plus[®] results also in a dataset with conodes representing the phase behavior in the system with all intermediate species, hemiformals and methylene glycols of different chain lengths. These numbers can be stoichiometrically recalculated to the three-component mixture of W/MeOH/FA. Column C-2 comprises 50 stages, each of which is operated at vapor-liquid equilibrium with temperatures between 337–373 K. Feed is given between stages 8 and 9 with a stoichiometric composition of 40.7 wt.-% water, 40.7 wt.-% FA and 18.6 wt.-% methanol (see formalin I in Table 10).

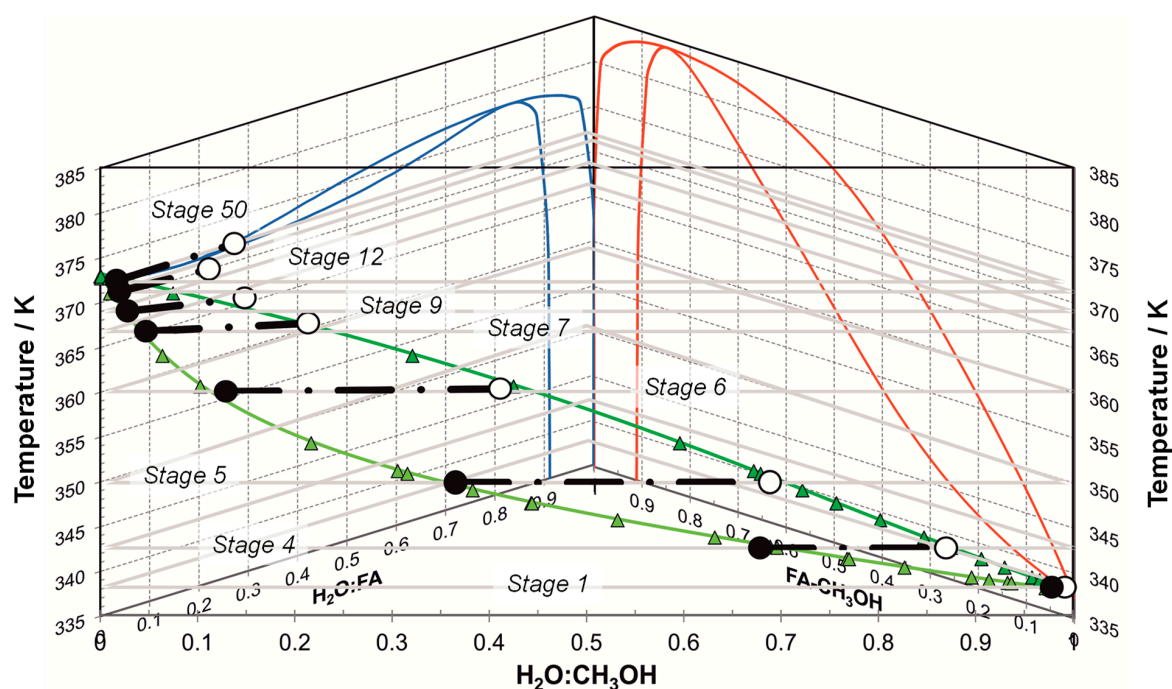


Figure 11. Illustration of the phase equilibria W/MeOH/FA with experimental literature data [80] and condones of selected stages in column C-2; see Figure 10.

As can be seen from Figure 11, only 8 stages between 337–367 K are necessary to obtain methanol of high purity at the top of the column, i.e., 99%. These condones are placed at the front of the 3D-prism, $T(x_W, x_{MeOH})$, and were determined by the binary methanol-water system. In contrast, 40 stages are required to achieve a 50:50 (by weight) W/FA solution (formalin II) at the bottom of the column. The temperature change from stage to stage is very small due to the narrow band between the liquid and gaseous phases. The condones are placed on the back side of the 3D-prism, $T(x_W, x_{FA})$, and were determined by the binary W/FA system. Finally, it can be stated that the design of the distillation column leads to mixtures in a small space within the complete phase diagram. Solid precipitation should not play a role in this composition matrix.

Process Assessment

Table 10 lists the three different cases of the simulation using different absorbents and having different target products, corresponding to the OME₃₋₅ synthesis routes shown in Figure 9. In accordance with the stoichiometric compositions listed in Table 10, Figures 12 and 13 show the true compositions of the chemical equilibrium at 60 °C and 1 bar in weight and molar fraction, respectively. As formalin II contains almost no methanol, no HF_n is formed. The true water contents at 60 °C and 1 bar of 34.2 wt.-% (66.8 mol.-%) in the case of formalin I and 34.9 wt.-% (69.8 mol.-%) in the case of formalin II are not shown in Figures 12 and 13.

Table 10. Products of formalin synthesis using different absorbents.

Product	Stoichiometric Weight Fraction/wt.-%			Route	Absorbent
	FA	Water	Methanol		
Formalin Ia	40.7	40.7	18.6	A	Freshwater
Formalin Ib	40.7	40.7	18.6	B	OME ₁ wastewater (5.0 wt.-% FA)
Formalin II	50.0	50.0	0.0	B, C	TRI wastewater (1.0 wt.-% FA)

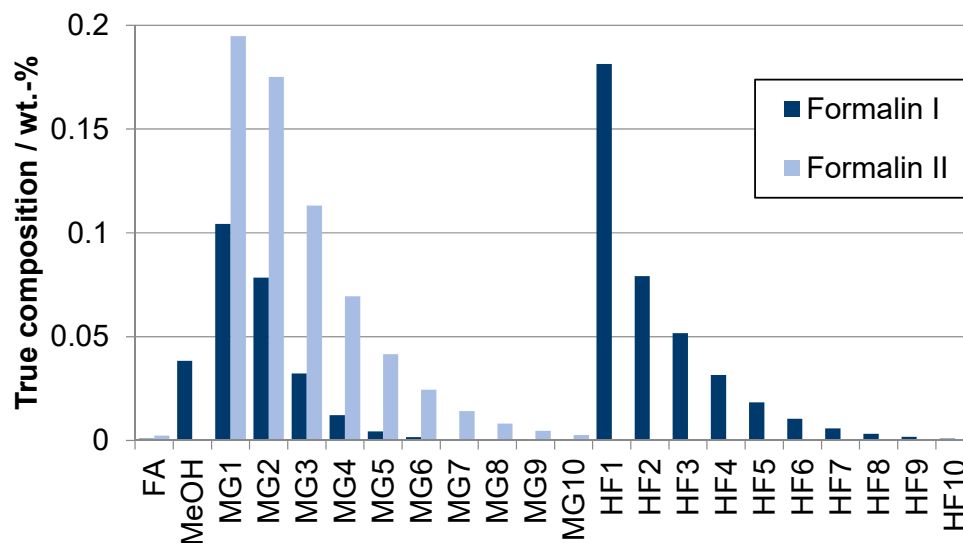


Figure 12. True composition in weight as a percentage of formalin I and formalin II at 60 °C and 1 bar.

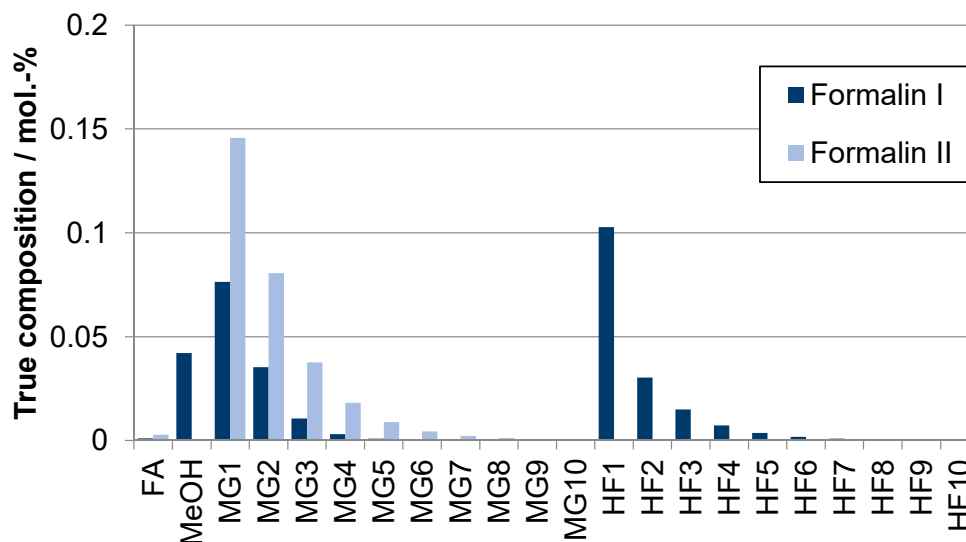


Figure 13. True composition in molar percent of formalin I and formalin II at 60 °C and 1 bar.

Table 11 displays the utility demand. Water cooling is not required, as cooling is provided via steam generation or air cooling. As the entire process runs at atmospheric pressure and pressure losses are neglected in this case study, no electricity demand is listed in Table 11. The distillation separation in column C-2 (see Figure 10) requires a comparatively higher amount of thermal energy (see Table 11) to ensure a high purity (99.9 wt.-% FA+W) of formalin for the downstream trioxane synthesis. The preheating of the feed using the heat exchanger E-8 is limited, as the formalin II stream can only be cooled to 60 °C because long-chain MG_n could otherwise precipitate as solids [28].

The use of the wastewater of the OME_1 synthesis as the absorbent in column C-1 decreases the methanol content of the absorber tail gas, slightly reducing the steam generated by tail gas burning. The amount of steam generated by formalin II synthesis is higher, as formalin II is methanol-free. This also reduces the raw material of methanol. The formalin II synthesis requires $0.706 \text{ kg}_{MeOH}/\text{kg}_{FA}$, whereas the syntheses of formalin Ia and formalin Ib require $0.763 \text{ kg}_{MeOH}/\text{kg}_{FA}$ and $0.740 \text{ kg}_{MeOH}/\text{kg}_{FA}$.

As reported by Schemme et al. [11], using the wastewater from the OME_1 synthesis plant as the absorbent in the upstream formalin synthesis leads, with the chosen assumptions, to an increase in the power-to-fuel efficiency from $\eta_{PTL} = 0.443$ to $\eta_{PTL} = 0.448$. The H_2 demand and CO_2 demand drop from $0.275 \text{ kg}_{H_2}/\text{kg}_{OME_1}$ to $0.270 \text{ kg}_{H_2}/\text{kg}_{OME_1}$ and from $3.039 \text{ kg}_{CO_2}/\text{l}_{DE}$ to $2.987 \text{ kg}_{CO_2}/\text{l}_{DE}$, respectively [11].

Table 11. Heat demand and excess of formalin synthesis from methanol. HP: high pressure (39.7 bar), MP: medium pressure (8.9 bar) and LP: low pressure (2.3 bar).

Unit	Formalin Ia Heat MJ/kg	Formalin Ib Heat MJ/kg	Formalin II Heat MJ/kg	Temperature Level °C	Heating or Cooling Utility
Reactor R-1	-2.183	-2.119	-2.665	630	HP steam (250 °C)
Steam generator E-5	-1.964	-1.830	-2.385	260	HP steam (250 °C)
Steam generator E-6	-0.264	-0.256	-0.322	185	MP steam (175 °C)
Steam generator E-7	-0.174	-0.168	-0.212	135	LP steam (125 °C)
Column Reboiler C-2	-	-	4.892	99	LP steam (125 °C)

4. Conclusions

In this work, the deviation between the calculated results using thermodynamic models and experimental literature data was determined using commercial spreadsheet software (Microsoft® Excel) and process simulation software (Aspen Plus®). In the latter case, the standard deviation was reduced to less than 4.9% in worst case by means of a curve-fitting method. Previously, the equations of the original model were adjusted through parameter-fitting to be used in the respective Aspen Plus® input template.

Aside from the physico-chemical behavior of the component system, reliable property data is fundamental for sound process simulations. However, important substances (polyoxymethylene dimethyl ethers (OME_{n>1}), hemiformals (HF_n) and methylene glycols (MG_n)) that take place in the OME₃₋₅ synthesis are not available in the databases of common process simulation software like Aspen Plus® or CHEMCAD. Missing property data can be estimated based on the molecular structure using group contribution methods, whereby the accuracy of the prediction can be significantly improved when the normal boiling points (T_B) are given. However, the T_B of HF_n and MG_n cannot normally be physically measured, as these substances do not exist in pure form.

This study also determined the normal boiling points (T_B) of HF₂₋₁₀ and MG₂₋₁₀ based on molecular analogies to OME_n. The T_B of OME₁ is given in the Aspen Plus® database, and while the T_B of OME₂₋₅ can be calculated using values from the literature. The T_B of OME_n was determined extrapolating the vapor pressure equation parameters of OME₂₋₅.

As an example of its application, we demonstrated herein that an optimization of the state-of-the-art formaldehyde synthesis process is possible based on the developed approaches, inter alia, along the OME₃₋₅ synthesis routes. As different formaldehyde solutions along the synthesis routes are required, different process variations are presented in the optimization. Using the wastewater from subsequent processes as the absorbent in the FA synthesis, the loss of methanol in the absorber flue gas and the loss of formaldehyde in the wastewater were significantly reduced. In the case presented, using the wastewater of the OME₁ synthesis decreases the demand of H₂ from 0.275 kg_{H2}/kg_{OME1} to 0.270 kg_{H2}/kg_{OME1} and the demand of CO₂ from 3.039 kg_{CO2}/l_{DE} to 2.987 kg_{CO2}/l_{DE}. Overall, the power-to-fuel efficiency can be improved by 0.5 percentage points using the suggested approach. Finally, the proposed modelling approach in this paper opens the way to further process optimization studies for the rather complex synthesis routes to produce OME₃₋₅.

Author Contributions: Conceptualization, S.S., R.C.S. and R.P.; methodology, S.S. and R.P.; software, S.M. and M.K.; validation, S.M., M.K. and S.S.; investigation, S.S.; writing—original draft preparation, S.S.; writing—review and editing, S.S., R.C.S., and R.P.; visualization, S.S. and R.P.; supervision, R.C.S., R.P. and D.S.; project administration, R.P.; funding acquisition, R.P., D.S. All authors have read and agreed to the published version of the manuscript.

Funding: This research was partly funded by ACT ALIGN-CCUS Project, grant number 271501 and partly performed within the framework of project house TESYS (Technology-based Energy Systems Analysis) of RWTH

Aachen University, financed by the Excellence Initiative of the German federal and state governments to promote science and research at German universities.

Acknowledgments: The authors would like to thank the members of the group “Future Fuels” at the Forschungszentrum Jülich GmbH, Institute of Energy and Climate Research (IEK-14 – Electrochemical Process Engineering) for their valuable input. Further thanks are addressed to the members of the JARA Energy seed fund, “Power to Fuel,” and its successor – The Competence Center Power to Fuel. JARA (Jülich-Aachen Research Alliance) is an initiative of RWTH Aachen University and the Forschungszentrum Jülich. This work was funded in part by the ACT ALIGN-CCUS Project No. 271501. Additionally, this work was partly performed within the framework of project house TESYS (Technology-based Energy Systems Analysis) of RWTH Aachen University, financed by the Excellence Initiative of the German federal and state governments to promote science and research at German universities.

Conflicts of Interest: The authors declare no conflict of interest. The funders had no role in the design of the study; in the collection, analyses, or interpretation of data; in the writing of the manuscript, or in the decision to publish the results.

Abbreviations

FA	Formaldehyde
W	Water
MeOH	Methanol
MG	Methylene glycol
OME ₁	Methylal
OME	Polyoxymethylen dimethylether
HF	Hemiformal
TRI	Trioxane
DME	Dimethyl ether
T _B	Normal boiling point
T _C	Critical temperature
P _C	Critical pressure
ARD	Average of the relative deviations
s	Standard deviation
STP	Standard temperature and pressure
ΔG_R	Gibbs free energy
ΔH_R	Enthalpy of reaction

Appendix A

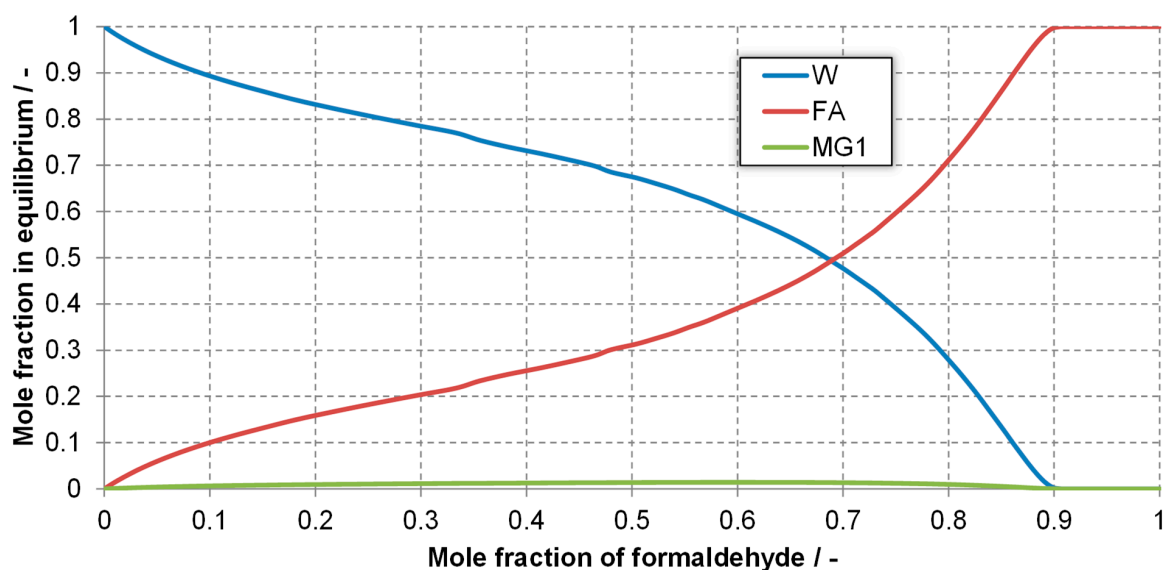


Figure A1. Equilibrium distribution in the gas phase of the component system FA-W at 90 °C.

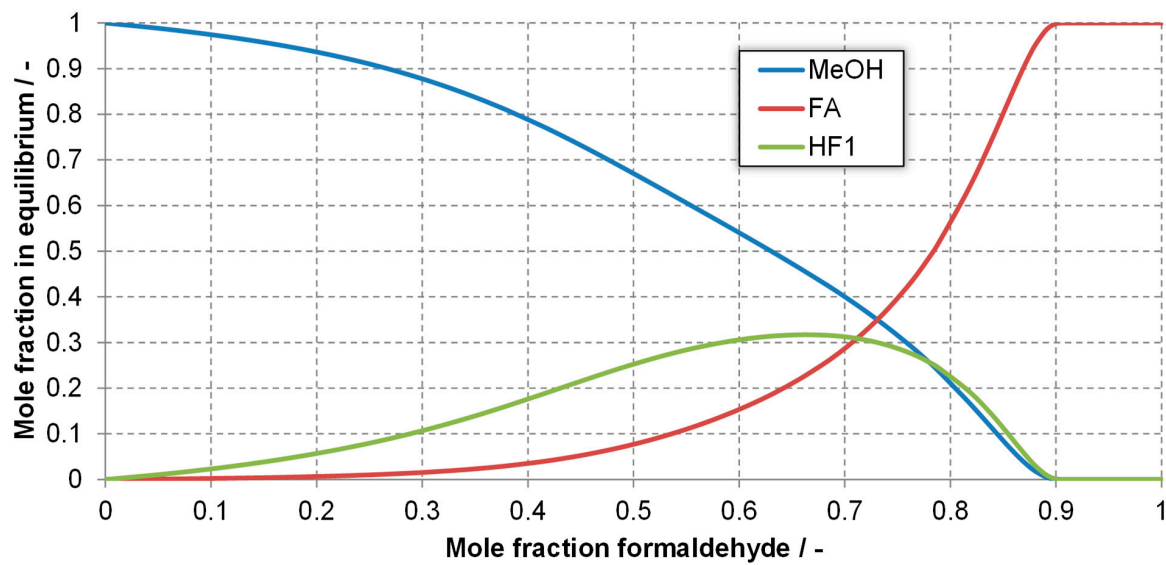


Figure A2. Equilibrium distribution in the gas phase of the component system FA-MeOH at 80 °C.

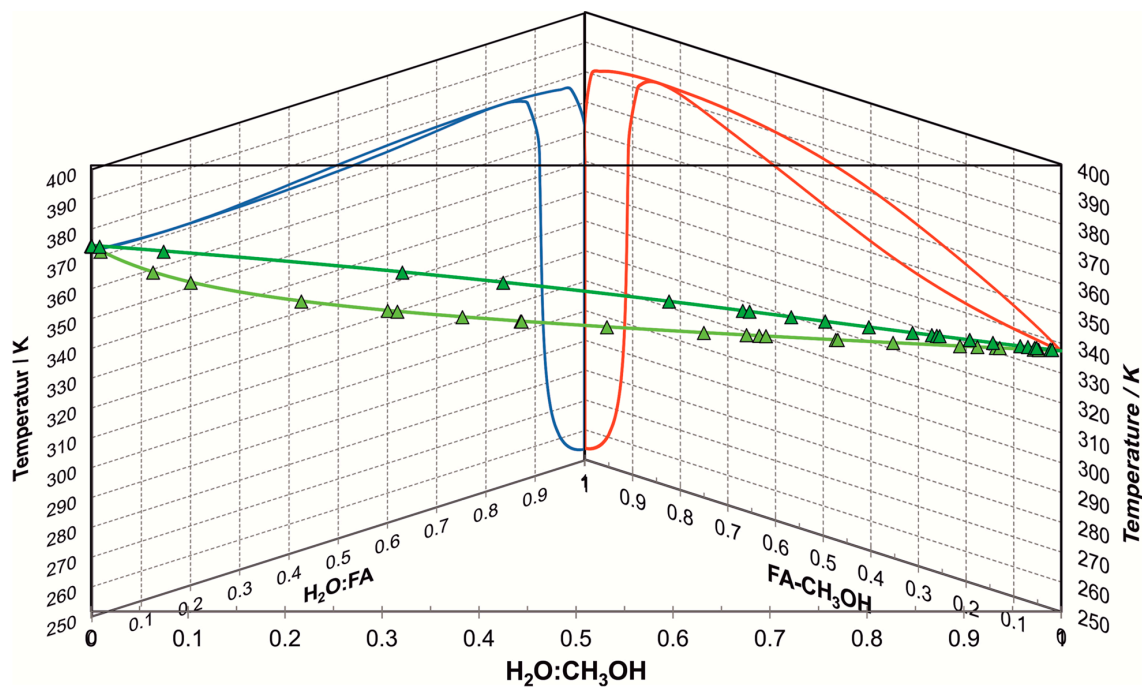


Figure A3. Prism illustration of temperature-dependent binary diagrams of the system W/MeOH/FA.

Appendix A.1 Model for Activity-Based Equilibrium Constants

The correlations for K_{MG_1} and K_{HF_1} (Equations (A1) and (A2)) refer to the gas phase and all others to the liquid phase. The corresponding conversion between the gas and liquid phases takes place via the vapor pressures [32]:

$$K_{MG_1}^L = \frac{x_{MG_1}}{x_W x_{FA}} \frac{\gamma_{MG_1}}{\gamma_W \gamma_{FA}} = K_{MG_1}^G \frac{p_W^S p_{FA}^S}{p_{MG_1}^S p_0} \quad (\text{A1})$$

$$K_{HF_1}^L = \frac{x_{HF}}{x_{MeOH} x_{FA}} \frac{\gamma_{HF}}{\gamma_{MeOH} \gamma_{FA}} = K_{HF_1}^G \frac{p_{MeOH}^S p_{FA}^S}{p_{HF_1}^S p_0} \quad (\text{A2})$$

Equations (A3) und (A4) describe the equilibrium constants of longer HF_n and MG_n with n ≥ 2 [32]:

$$K_{MG_n}^L = \frac{x_{MG_n} x_W}{x_{MG_{n-1}} x_{MG_1}} \frac{\gamma_{MG_n} \gamma_W}{\gamma_{MG_{n-1}} \gamma_{MG_1}} \quad n \geq 2 \quad (A3)$$

$$K_{HF_n}^L = \frac{x_{HF_n} x_{MeOH}}{x_{HF_{n-1}} x_{HF_1}} \frac{\gamma_{HF_n} \gamma_{MeOH}}{\gamma_{HF_{n-1}} \gamma_{HF_1}} \quad n \geq 2 \quad (A4)$$

The mass balances (Equations (A5) to (A8)) given by Albert et al. [52] to recalculate the FA, W and MeOH shares are as follows:

$$\tilde{x}_{FA} = \frac{1}{s} \left[x_{FA} + \sum_{i=1}^{\infty} (i \cdot x_{MG_i}) + \sum_{i=1}^{\infty} (i \cdot x_{HF_i}) \right] \quad (A5)$$

$$\tilde{x}_W = \frac{1}{s} \left[x_W + \sum_{i=1}^{\infty} x_{MG_i} \right] \quad (A6)$$

$$\tilde{x}_{MeOH} = \frac{1}{s} \left[x_{MeOH} + \sum_{i=1}^{\infty} x_{HF_i} \right] \quad (A7)$$

$$s = 1 + \sum_{i=1}^{\infty} (i \cdot x_{MG_i}) + \sum_{i=1}^{\infty} (i \cdot x_{HF_i}) \quad (A8)$$

Appendix A.2 UNIFAC Parameters Required for Modeling Component Systems on OME₃₋₅ Synthesis Routes

Table A1. NRTL parameters of the component system trioxane-methylal and UNIFAC interaction parameters determined by data regression.

NRTL Parameter [21]		UNIFAC Parameter (Regression)	
<i>a</i> _{TRI,DMM}	0.3	Ψ _{(CH₂O)₃,C₃H₈O₂}	142.2
<i>a</i> _{DMM,TRI}	0.3	Ψ _{C₃H₈O₂,(CH₂O)₃}	-22.0
<i>b</i> _{TRI,DMM}	251.45	-	-
<i>b</i> _{DMM,TRI}	33.22	-	-

Table A2. UNIFAC groups.

Substance	Molecule Groups		Reference
Water	H ₂ O		[32]
Formaldehyde	CH ₂ O		[32]
Methanol	CH ₃ OH		[32]
MG ₁	CH ₂ (OH) ₂		[32]
MG ₂₋₁₀	(n - 1)	-CH ₂ O-	[32]
	2	-OH	
	1	-CH ₂ -	
HF ₁₋₁₀	(n - 1)	-CH ₂ O-	[32]
	1	CH ₃ O-	
	1	-CH ₂ OH	
Trioxane	(CH ₂ O) ₃		Grützner [72] (based on Albert [49])
Methylal	C ₃ H ₈ O ₂		Drunsel [29] (based on Kuhnert [73])
Dimethylether	1	C ₂ H ₆ O	assumption
OME ₂₋₁₀	n	(CH ₂ O) _{OME}	[54]
	1	C ₃ H ₈ O ₂	

Table A3. UNIFAC volume and surface parameters.

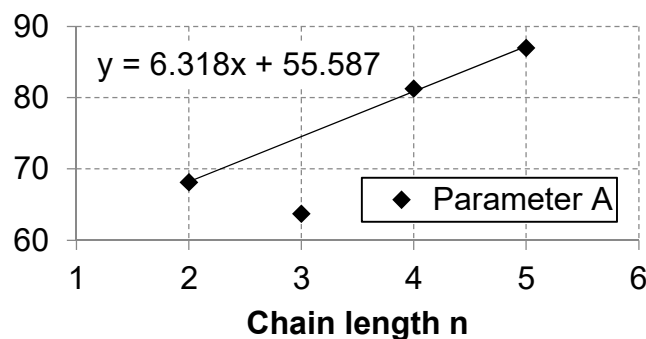
Number	Molecule Group	R	Q	Reference
1	-OH	1.0	1.2	[32]
2	-CH ₂ O-	0.9183	0.78	[32]
3	(CH ₂ O) _{OME}	0.9183	0.78	[54]
4	-CH ₂ -	0.6744	0.54	[32]
5	-CH ₃	0.9011	0.848	[43]
6	H ₂ O	0.9200	1.4	[32]
7	CH ₂ (OH) ₂	2.6744	2.94	[32]
8	CH ₃ OH	1.4311	1.432	[32]
9	CH ₃ O-	1.1450	1.088	[32]
10	-CH ₂ OH	1.2044	1.124	[32]
11	(CH ₂ O) ₃	2.754	2.34	Grützner [72] (based on Albert [49])
12	C ₃ H ₈ O ₂	2.9644	2.716	Drunsel [29] (based on Kuhnert [73])
13	C ₂ H ₆ O	1.23	0.418	regression

Table A4. Interaction parameters Ψ_{ij} of the UNIFAC groups listed in Tables A2 and A3.

i\j	1	2	4/5	6	7	8	9	10	11	12	13	3
1	0.0	28.1	156.4	353.5	353.5	-137.1	28.1	-137.1	28.1	28.1	0.0	28.1
2	237.7	0.0	83.4	240.0	240.0	339.7	0.0	339.7	-320.6 *	0.0	0.0	0.0
4/5	986.5	251.5	0.0	1318.0	1318.0	697.2	251.5	697.2	251.5	251.5	0.0	251.5
6	-229.1	-149.0	300.0	0.00	0.0	289.6	-149.0	289.6	80.6	28.9 *	79.6	-141.0 *
7	-229.1	-149.0	300.0	0.00	0.0	289.6	-149.0	289.6	80.6	28.9 *	0.0	-149.0
8	249.1	-180.6	16.5	-181.0	-181.0	0.0	-180.6	0.0	-16.7	-71.2	-69.4	-180.6
9	237.7	0.0	83.4	240.0	240.0	339.7	0.0	339.7	0.00	0.0	0.0	0.0
10	249.1	-180.6	16.5	-181.0	-181.0	0.0	-180.6	0.0	-187.7	0.0	0.0	-180.6
11	237.7	3041.2 *	83.4	379.4	379.4	239.6	0.0	392.2	0.00	142.2	0.0	3041.2 *
12	237.7	0.0	83.4	413.4 *	413.3 *	410.0	0.0	0.0	-22.0	0.0	0.0	26.0
13	0.0	0.0	0.0	-447.5	0.0	-364.1	0.0	0.0	0.0	0.0	0.0	0.0
3	237.7	0.0	83.4	670.7	240.0	339.7	0.0	339.7	-320.6 *	141.5	0.0	0.0

* for T = 80 °C.

Appendix A.3 Linear Regression of Correlations Parameters

**Figure A4.** Linear regression of correlation parameter A of the vapor pressure equation (Equation (8)) for OME₂₋₅ (data given by Boyd [77]).

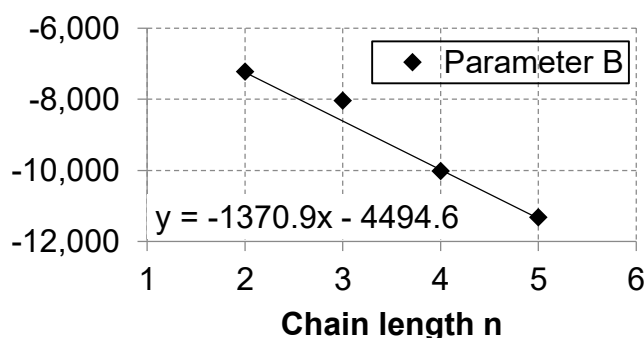


Figure A5. Linear regression of correlation parameter B of the vapor pressure equation (Equation (8)) for OME₂₋₅ (data given by Boyd [77]).

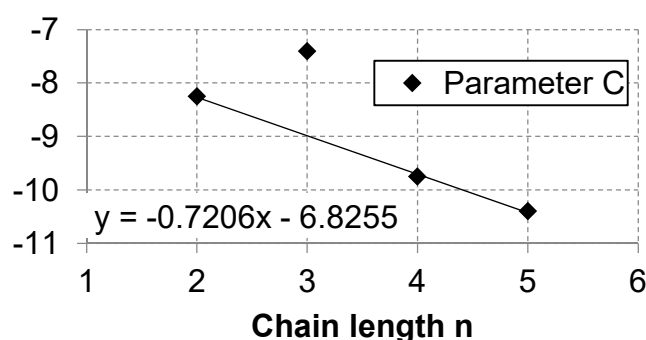


Figure A6. Linear regression of correlation parameter C of the vapor pressure equation (Equation (8)) for OME₂₋₅ (data given by Boyd [77]).

Table A5. Normal boiling points of MG₁₋₁₀ and HF₁₋₁₀ based on the molecular structure using the group contribution method PCES (not to be used; the values used are listed in Table 7).

T _B /°C	n = 1	n = 2	n = 3	n = 4	n = 5	n = 6	n = 7	n = 8	n = 9	n = 10
MG _n	133.5	178.8	224.1	269.4	314.7	360.0	405.3	450.6	495.9	541.2
HF _n	86.6	131.9	177.2	222.5	267.8	313.1	358.4	403.7	449.0	494.3

References

- Schemme, S.; Samsun, R.C.; Peters, R.; Stolten, D. Power-to-fuel as a key to sustainable transport systems—An analysis of diesel fuels produced from CO₂ and renewable electricity. *Fuel* **2017**, *205*, 198–221. [[CrossRef](#)]
- Lumpp, B.; Rothe, D.; Pastötter, C.; Lämmermann, R.; Jacob, E. Oxymethylene Ethers as Diesel Fuel Additives of the Future. *MTZ Worldwide eMagazine* **2011**, *72*, 34–38. [[CrossRef](#)]
- Burger, J.; Siegert, M.; Ströfer, E.; Hasse, H. Poly(oxymethylene) dimethyl ethers as components of tailored diesel fuel: Properties, synthesis and purification concepts. *Fuel* **2010**, *89*, 3315–3319. [[CrossRef](#)]
- Lautenschütz, L.; Oestreich, D.; Seidenspinner, P.; Arnold, U.; Dinjus, E.; Sauer, J. Physico-chemical properties and fuel characteristics of oxymethylene dialkyl ethers. *Fuel* **2016**, *173*, 129–137. [[CrossRef](#)]
- Barro, C.; Parravicini, M.; Boulouchos, K. Neat polyoxymethylene dimethyl ether in a diesel engine; part 1: Detailed combustion analysis. *Fuel* **2019**, *256*, 115892. [[CrossRef](#)]
- Iannuzzi, S.E.; Barro, C.; Boulouchos, K.; Burger, J. POMDME-diesel blends: Evaluation of performance and exhaust emissions in a single cylinder heavy-duty diesel engine. *Fuel* **2017**, *203*, 57–67. [[CrossRef](#)]
- Omari, A.; Heuser, B.; Pischinger, S. Potential of oxymethylenether-diesel blends for ultra-low emission engines. *Fuel* **2017**, *209*, 232–237. [[CrossRef](#)]
- Härtl, M.; Seidenspinner, P.; Jacob, E.; Wachtmeister, G. Oxygenate screening on a heavy-duty diesel engine and emission characteristics of highly oxygenated oxymethylene ether fuel OME1. *Fuel* **2015**, *153*, 328–335. [[CrossRef](#)]

9. Zimmermann, A.W.; Gençer, E.; O'Sullivan, F.; Schmäckera, R. E-fuels as Carbon Capture and Utilization Option for the Industry? A Standardized Techno-Economic Assessment OME3–5. In Proceedings of the 14th International Conference on Greenhouse Gas Control Technologies, GHGT-14, Melbourne, Australia, 22–25 October 2018.
10. Bongartz, D.; Burre, J.; Mitsos, A. Production of Oxymethylene Dimethyl Ethers from Hydrogen and Carbon Dioxide—Part I: Modeling and Analysis for OME1. *Ind. Eng. Chem. Res.* **2019**, *58*, 4881–4889. [[CrossRef](#)]
11. Schemme, S.; Breuer, J.L.; Köller, M.; Meschede, S.; Walman, F.; Samsun, R.C.; Peters, R.; Stolten, D. H₂-based synthetic fuels: A techno-economic comparison of alcohol, ether and hydrocarbon production. *Int. J. Hydrogen Energy* **2019**, *45*, 5395–5414. [[CrossRef](#)]
12. Held, M.; Tönges, Y.; Pélerin, D.; Härtl, M.; Wachtmeister, G.; Burger, J. On the energetic efficiency of producing polyoxymethylene dimethyl ethers from CO₂ using electrical energy. *Energy Environ. Sci.* **2019**, *12*, 1019–1034. [[CrossRef](#)]
13. Burre, J.; Bongartz, D.; Mitsos, A. Production of Oxymethylene Dimethyl Ethers from Hydrogen and Carbon Dioxide—Part II: Modeling and Analysis for OME3–5. *Ind. Eng. Chem. Res.* **2019**, *58*, 5567–5578. [[CrossRef](#)]
14. Breitzkreuz, C.F.; Schmitz, N.; Ströfer, E.; Burger, J.; Hasse, H. Design of a Production Process for Poly(oxymethylene) Dimethyl Ethers from Dimethyl Ether and Trioxane. *Chemie Ingenieur Technik* **2018**, *90*, 1–9. [[CrossRef](#)]
15. Schmitz, N.; Burger, J.; Ströfer, E.; Hasse, H. From methanol to the oxygenated diesel fuel poly(oxymethylene) dimethyl ether: An assessment of the production costs. *Fuel* **2016**, *185*, 67–72. [[CrossRef](#)]
16. Ouda, M.; Mantei, F.K.; Elmehlawy, M.; White, R.J.; Klein, H.; Fateen, S.E.K. Describing oxymethylene ether synthesis based on the application of non-stoichiometric Gibbs minimisation. *React. Chem. Eng.* **2018**, *3*, 277–292. [[CrossRef](#)]
17. Peters, R. Identification and thermodynamic analysis of reaction pathways of methylal and OME-n formation. *Energy* **2017**, *138*, 1221–1246. [[CrossRef](#)]
18. Peters, R.; Decker, M.; Eggemann, L.; Schemme, S.; Schorn, F.; Breuer, J.L.; Weiske, S.; Pasel, J.; Samsun, R.C.; Stolten, D. Thermodynamic and ecological preselection of synthetic fuel intermediates from biogas at farm sites. *Energy Sustain. Soc.* **2020**, *10*, 4. [[CrossRef](#)]
19. Baranowski, C.J.; Bahmanpour, A.M.; Kröcher, O. Catalytic synthesis of polyoxymethylene dimethyl ethers (OME): A review. *Appl. Catal. B Environ.* **2017**, *217*, 407–420. [[CrossRef](#)]
20. Hackbarth, K.; Haltenort, P.; Arnold, U.; Sauer, J. Recent Progress in the Production, Application and Evaluation of Oxymethylene Ethers. *Chemie Ingenieur Technik* **2018**, *90*, 1–10. [[CrossRef](#)]
21. Burger, J. A Novel Process for the Production of Diesel Fuel Additives by Hierarchical Design. Ph.D. Thesis, Kaiserslautern Technical University, Kaiserslautern, Germany, 2012.
22. Oestreich, D. Prozessentwicklung zur Gewinnung von Oxymethylenethern (OME) aus Methanol und Formaldehyd. Ph.D. Thesis, Karlsruher Institut für Technology, Karlsruhe, Germany, 2017.
23. Bhatelia, T.; Lee, W.J.; Samanta, C.; Patel, J.; Bordoloi, A. Processes for the production of oxymethylene ethers: Promising synthetic diesel additives. *Asia-Pac. J. Chem. Eng.* **2017**, *12*, 827–837. [[CrossRef](#)]
24. Weidert, J.-O.; Burger, J.; Renner, M.; Blagov, S.; Hasse, H. Development of an Integrated Reaction–Distillation Process for the Production of Methylal. *Ind. Eng. Chem. Res.* **2017**, *56*, 575–582. [[CrossRef](#)]
25. Schmitz, N.; Strofer, E.; Burger, J.; Hasse, H. Conceptual Design of a Novel Process for the Production of Poly(oxymethylene) Dimethyl Ethers from Formaldehyde and Methanol. *Ind. Eng. Chem. Res.* **2017**, *56*, 11519–11530. [[CrossRef](#)]
26. Schmitz, N.; Breitzkreuz, C.F.; Ströfer, E.; Burger, J.; Hasse, H. Separation of water from mixtures containing formaldehyde, water, methanol, methylal, and poly(oxymethylene) dimethyl ethers by pervaporation. *J. Membr. Sci.* **2018**, *564*, 806–812. [[CrossRef](#)]
27. Bertau, M.; Räuchle, K.; Offermanns, H. Methanol—Die Basischemikalie. *Chemie In Unserer Zeit* **2015**, *49*, 312–329. [[CrossRef](#)]
28. Reuss, G.; Disteldorf, W.; Gamer, A.O.; Hilt, A. Formaldehyde. In *Ullmann's Encyclopedia of Industrial Chemistry*; Wiley-VCH Verlag GmbH & Co. KGaA: Weinheim, Germany, 2012; Volume 15. [[CrossRef](#)]
29. Drunsel, J.-O.; Renner, M.; Hasse, H. Experimental study and model of reaction kinetics of heterogeneously catalyzed methylal synthesis. *Chem. Eng. Res. Des.* **2012**, *90*, 696–703. [[CrossRef](#)]

30. Hahnenstein, I.; Albert, M.; Hasse, H.; Kreiter, C.G.; Maurer, G. NMR Spectroscopic and Densimetric Study of Reaction Kinetics of Formaldehyde Polymer Formation in Water, Deuterium Oxide, and Methanol. *Ind. Eng. Chem. Res.* **1995**, *34*, 440–450. [[CrossRef](#)]
31. Maiwald, M.; Fischer, H.H.; Ott, M.; Peschla, R.; Kuhnert, C.; Kreiter, C.G.; Maurer, G.; Hasse, H. Quantitative NMR Spectroscopy of Complex Liquid Mixtures: Methods and Results for Chemical Equilibria in Formaldehyde–Water–Methanol at Temperatures up to 383 K. *Ind. Eng. Chem. Res.* **2003**, *42*, 259–266. [[CrossRef](#)]
32. Maurer, G. Vapor-Liquid Equilibrium of Formaldehyde- and Water-Containing Multicomponent Mixtures. *AIChE J.* **1986**, *32*, 932–948. [[CrossRef](#)]
33. Kuhnert, C.; Albert, M.; Breyer, S.; Hahnenstein, I.; Hasse, H.; Maurer, G. Phase Equilibrium in Formaldehyde Containing Multicomponent Mixtures: Experimental Results for Fluid Phase Equilibria of (Formaldehyde + (Water or Methanol) + Methylal) and (Formaldehyde + Water + Methanol + Methylal) and Comparison with Predictions. *Ind. Eng. Chem. Res.* **2006**, *45*, 5155–5164. [[CrossRef](#)]
34. Albert, M.; García, B.C.; Kreiter, C.; Maurer, G. Vapor-liquid and chemical equilibria of formaldehyde-water mixtures. *AIChE J.* **1999**, *45*, 2024–2033. [[CrossRef](#)]
35. Albert, M.; Hasse, H.; Kuhnert, C.; Maurer, G. New Experimental Results for the Vapor–Liquid Equilibrium of the Binary System (Trioxane + Water) and the Ternary System (Formaldehyde + Trioxane + Water). *J. Chem. Eng. Data* **2005**, *50*, 1218–1223. [[CrossRef](#)]
36. Albert, M.; Hahnenstein, I.; Hasse, H.; Maurer, G. Vapor–liquid equilibrium of formaldehyde mixtures: New data and model revision. *AIChE J.* **1996**, *42*, 1741–1752. [[CrossRef](#)]
37. Ott, M.; Schoenmakers, H.; Hasse, H. Distillation of formaldehyde containing mixtures: Laboratory experiments, equilibrium stage modeling and simulation. *Chem. Eng. Process. Process Intensif.* **2005**, *44*, 687–694. [[CrossRef](#)]
38. Grützner, T.; Hasse, H. Solubility of Formaldehyde and Trioxane in Aqueous Solutions. *J. Chem. Eng. Data* **2004**, *49*, 642–646. [[CrossRef](#)]
39. O’Connell, J.P.; Gani, R.; Mathias, P.M.; Maurer, G.; Olson, J.D.; Crafts, P.A. Thermodynamic Property Modeling for Chemical Process and Product Engineering: Some Perspectives. *Ind. Eng. Chem. Res.* **2009**, *48*, 4619–4637. [[CrossRef](#)]
40. Grützner, T.; Hasse, H.; Lang, N.; Siegert, M.; Ströfer, E. Development of a new industrial process for trioxane production. *Chem. Eng. Sci.* **2007**, *62*, 5613–5620. [[CrossRef](#)]
41. Ouda, M.; Yarce, G.; White, R.J.; Hadrich, M.; Himmel, D.; Schaadt, A.; Klein, H.; Jacob, E.; Krossing, I. Poly(oxyethylene) dimethyl ether synthesis—A combined chemical equilibrium investigation towards an increasingly efficient and potentially sustainable synthetic route. *React. Chem. Eng.* **2017**, *2*, 50–59. [[CrossRef](#)]
42. Schmitz, N.; Breitzkreuz, C.F.; Ströfer, E.; Burger, J.; Hasse, H. Vapor–liquid equilibrium and distillation of mixtures containing formaldehyde and poly(oxyethylene) dimethyl ethers. *Chem. Eng. Process. Process Intensif.* **2018**, *131*, 116–124. [[CrossRef](#)]
43. Fredenslund, A.; Jones, R.L.; Prausnitz, J.M. Group-contribution estimation of activity coefficients in nonideal liquid mixtures. *AIChE J.* **1975**, *21*, 1086–1099. [[CrossRef](#)]
44. Joback, K.G.; Reid, R.C. Estimation of pure-component properties from group-contributions. *Chem. Eng. Commun.* **1987**, *57*, 233–243. [[CrossRef](#)]
45. Constantinou, L.; Gani, R. New group contribution method for estimating properties of pure compounds. *AIChE J.* **1994**, *40*, 1697–1710. [[CrossRef](#)]
46. Aspen Technology, I. Aspen Physical Property System. In *Physical Property Methods and Models*; Aspen Technology: Cambridge, MA, USA, 2001.
47. Gmehling, J.; Rasmussen, P.; Fredenslund, A. Vapor-liquid equilibria by UNIFAC group contribution. Revision and extension. 2. *Ind. Eng. Chem. Process Des. Dev.* **1982**, *21*, 118–127. [[CrossRef](#)]
48. Hahnenstein, I.; Hasse, H.; Kreiter, C.G.; Maurer, G. ¹H- and ¹³C-NMR-Spectroscopic Study of Chemical Equilibria in Solutions of Formaldehyde in Water, Deuterium Oxide, and Methanol. *Ind. Eng. Chem. Res.* **1994**, *33*, 1022–1029. [[CrossRef](#)]
49. Albert, M. Thermodynamische Eigenschaften formaldehydhaltiger Mischungen. Ph.D. Thesis, Universität Kaiserslautern, Aachen, Germany, 1999.
50. Hasse, H.; Hahnenstein, I.; Maurer, G. Revised vapor-liquid equilibrium model for multicomponent formaldehyde mixtures. *AIChE J.* **1990**, *36*, 1807–1814. [[CrossRef](#)]

51. Hasse, H.; Maurer, G. Vapor—Liquid equilibrium of formaldehyde-containing mixtures at temperatures below 320 K. *Fluid Phase Equilibria* **1991**, *64*, 185–199. [[CrossRef](#)]
52. Albert, M.; Coto García, B.; Kuhnert, C.; Peschla, R.; Maurer, G. Vapor–liquid equilibrium of aqueous solutions of formaldehyde and methanol. *AIChE J.* **2000**, *46*, 1676–1687. [[CrossRef](#)]
53. Albert, M.; Hahnenstein, I.; Hasse, H.; Maurer, G. Vapor–Liquid and Liquid–Liquid Equilibria in Binary and Ternary Mixtures of Water, Methanol, and Methylal. *J. Chem. Eng. Data* **2001**, *46*, 897–903. [[CrossRef](#)]
54. Schmitz, N.; Friebel, A.; von Harbou, E.; Burger, J.; Hasse, H. Liquid-liquid equilibrium in binary and ternary mixtures containing formaldehyde, water, methanol, methylal, and poly(oxyethylene) dimethyl ethers. *Fluid Phase Equilibria* **2016**, *425*, 127–135. [[CrossRef](#)]
55. Kuhnert, C.; Albert, M.; Breyer, S.; Hahnenstein, I.; Hasse, H.; Maurer, G. Phase Equilibrium in Formaldehyde Containing Multicomponent Mixtures: Experimental Results for Fluid Phase Equilibria of (Formaldehyde + (Water or Methanol) + Methylal) and (Formaldehyde + Water + Methanol + Methylal) and Comparison with Predictions. *Ind. Eng. Chem. Res.* **2006**, *45*, 6093–6094. [[CrossRef](#)]
56. Hasse, H.; Maurer, G. Kinetics of the poly(oxyethylene) glycol formation in aqueous formaldehyde solutions. *Ind. Eng. Chem. Res.* **1991**, *30*, 2195–2200. [[CrossRef](#)]
57. Ott, M.; Fischer, H.H.; Maiwald, M.; Albert, K.; Hasse, H. Kinetics of oligomerization reactions in formaldehyde solutions: NMR experiments up to 373K and thermodynamically consistent model. *Chem. Eng. Process. Process Intensif.* **2005**, *44*, 653–660. [[CrossRef](#)]
58. Ott, M. Reaktionskinetik und Destillation formaldehydhaltiger Mischungen. Ph.D. Thesis, TU Kaiserslautern, Kaiserslautern, Germany, 2004.
59. Ouda, M.; Mantei, F.; Hesterwerth, K.; Bargiacchi, E.; Klein, H.; White, R.J. A hybrid description and evaluation of oxyethylene dimethyl ethers synthesis based on the endothermic dehydrogenation of methanol. *React. Chem. Eng.* **2018**, *3*, 676–695. [[CrossRef](#)]
60. Ai, Z.-J.; Chung, C.-Y.; Chien, I.L. DESIGN AND CONTROL OF POLY(OXYMETHYLENE) DIMETHYL ETHERS PRODUCTION PROCESS DIRECTLY FROM FORMALDEHYDE AND METHANOL IN AQUEOUS SOLUTIONS. *IFAC-PapersOnLine* **2018**, *51*, 578–583. [[CrossRef](#)]
61. Liu, Y.-Q.; Hasse, H.; Maurer, G. Enthalpy change on vaporization of aqueous and methanolic formaldehyde solutions. *AIChE J.* **1992**, *38*, 1693–1702. [[CrossRef](#)]
62. Burger, J.; Ströfer, E.; Hasse, H. Production process for diesel fuel components poly(oxyethylene) dimethyl ethers from methane-based products by hierarchical optimization with varying model depth. *Chem. Eng. Res. Des.* **2013**, *91*, 2648–2662. [[CrossRef](#)]
63. Hasse, H. Dampf-Flüssigkeits-Gleichgewichte, Enthalpien und Reaktionskinetik in formaldehydhaltigen Mischungen. Ph.D. Thesis, University of Kaiserslautern, Kaiserslautern, Germany, 1990.
64. Soboleva, O.D.; Kazakova, S.V.; Blazhin, Y.M.; Ogorodnikov, S.K. Liquid-Vapor Equilibrium in the Formaldehyde-Water System. *Zhurnal Prikladnoi Khimii* **1984**, *57*, 860–865.
65. Kogan, L.V.; Blazhin, Y.M.; Ogorodnikov, S.K.; Kafarov, V.V. Liquid-Vapor Equilibrium in the System Formaldehyde-Water (Thermodynamic Verification with Chemical Interaction in the Liquid Phase Taken into Account). *Zhurnal Prikladnoi Khimii* **1977**, *50*, 2682–2687.
66. Walker, J.F. *Formaldehyde*; Reinhold: New York, NY, USA, 1964.
67. Savchenko, V.I. Equilibrium in the reaction of trioxane formation in aqueous formaldehyde solutions. *Bull. Acad. Sci. USSR Div. Chem. Sci.* **1969**, *18*, 2449–2451. [[CrossRef](#)]
68. Balashov, A.L.; Krasnov, V.L.; Danov, S.M.; Chernov, A.Y.; Sulimov, A.V. Formation of Cyclic Oligomers in Concentrated Aqueous Solutions of Formaldehyde. *J. Struct. Chem.* **2001**, *42*, 398–403. [[CrossRef](#)]
69. Drunsel, J.-O. Entwicklung von Verfahren zur Herstellung von Methylal und Ethylal. Ph.D. Thesis, Kaiserslautern Technical University, Kaiserslautern, Germany, 2012.
70. Gauss, C.F. *Abhandlungen zur Methode der Kleinsten Quadrate*; P. Stankiewicz: Berlin, Germany, 1887.
71. Redlich, O.; Kwong, J.N.S. On the Thermodynamics of Solutions. V. An Equation of State. Fugacities of Gaseous Solutions. *Chem. Rev.* **1949**, *44*, 233–244. [[CrossRef](#)]
72. Grützner, T. Entwicklung eines destillationsbasierten Verfahrens zur Herstellung von Trioxan. Ph.D. Thesis, Institut für Technische Thermodynamik und Thermische Verfahrenstechnik, Universität Stuttgart, Stuttgart, Germany, 2007.
73. Kuhnert, C. Dampf-Flüssigkeits-Gleichgewichte in mehrkomponentigen formaldehydhaltigen Systemen. Ph.D. Thesis, Universität Kaiserslautern, Kaiserslautern, Germany, 2004.

74. Haltenort, P.; Hackbarth, K.; Oestreich, D.; Lautenschütz, L.; Arnold, U.; Sauer, J. Heterogeneously catalyzed synthesis of oxymethylene dimethyl ethers (OME) from dimethyl ether and trioxane. *Catal. Commun.* **2018**, *109*, 80–84. [[CrossRef](#)]
75. AspenTech. *Aspen Physical Property System—Physical Property Models*; AspenTech: Cambridge, MA, USA, 2012.
76. AspenTech. *Aspen Plus User Guide V10.2*; AspenTech: Cambridge, MA, USA, 2000.
77. Boyd, R.H. Some Physical Properties of Polyoxymethylene Dimethyl Ethers. *J. Polym. Sci.* **1961**, *50*, 133–141. [[CrossRef](#)]
78. Chauvel, A.; Lefebvre, G. *Petrochemical Processes*; Editions OPHRYS: Paris, France, 2001.
79. Panzer, E.; Emig, G. *Verfahrensoptimierung der technischen Formaldehydsynthese am Silberkatalysator*; Lehrstuhl für Technische Chemie I, Universität Erlangen-Nürnberg: Nürnberg, Germany, 2000.
80. Álvarez, V.H.; Mattedi, S.; Iglesias, M.; Gonzalez-Olmos, R.; Resa, J.M. Phase equilibria of binary mixtures containing methyl acetate, water, methanol or ethanol at 101.3 kPa. *Phys. Chem. Liq.* **2011**, *49*, 52–71. [[CrossRef](#)]



© 2020 by the authors. Licensee MDPI, Basel, Switzerland. This article is an open access article distributed under the terms and conditions of the Creative Commons Attribution (CC BY) license (<http://creativecommons.org/licenses/by/4.0/>).